We are IntechOpen,
the world's leading publisher of
Open Access books
Built by scientists, for scientists

6,300
Open access books available

171,000
International authors and editors

190M
Downloads

154
Countries delivered to

Our authors are among the

TOP 1%
most cited scientists

12.2%
Contributors from top 500 universities

Interested in publishing with us?
Contact book.department@intechopen.com

Numbers displayed above are based on latest data collected.
For more information visit www.intechopen.com

Laser Processing of Silicon for Synthesis of Better Biomaterials

Candace Colpitts and Amirkianoosh Kiani

Additional information is available at the end of the chapter

Abstract

The increasing demand for new biomaterials and fabrication methods provides an opportunity for silicon to solve current challenges in the field. Laser processing is becoming more common as the public begins to understand its simplicity and value. When an abundant material is paired with a reliable and economic fabrication method, biomedical devices can be created and improved. In this chapter, different laser parameters of the Nd:YAG laser are investigated and the topographic and physical trends are analyzed. The biocompatibility is assessed for scanning speed, line spacing, overlap number, pulse frequency, and laser power with the use of simulated body fluid (SBF) and fibroblast culturing (NIH 3T3). Not only can nanosecond pulses increase the biocompatibility of silicon by generating silicon oxide nanofibers, but the substrate becomes bioactive with the manipulation of cell interactions.

Keywords: silicon, nanofibers, Nd:YAG laser, fibroblasts

1. Introduction

Science fiction has motivated intelligent minds to enhance the quality of living for the last century. A well-known example in fantasy is bionic limbs controlled by the mind. Individuals who have lost or permanently damaged limbs can benefit from procuring an aesthetically pleasing and fully functioning bionic replacement to restore or improve their quality of life. The field of biomaterials engineering has been making monumental advances by producing devices such as biosensors, bioMEMS, and artificial hearts [1–3]. There is a continuous growth in population today, demanding the attention from biomedical fields to improve lifestyles and create better body functionality. Although current devices' interfaces with the human body have come a long way, there is still a long way to go in the fabrication methods of the required scaffolds.

This chapter outlines one single pathway of research done to broaden the opportunities in the biomaterials industry. The bioactivity of laser-treated silicon is investigated through the use of *in vitro* testing. This research investigates of the trends of different laser parameters, including power, frequency, scanning speed, line spacing, and overlap number.

1.1. Challenges in the biomaterials industry

The current challenges in the biomedical field include finding biocompatible and bioactive organic or inorganic materials and simplifying manufacturing processes. Devices that are implanted inside the body require materials that are biocompatible; the behavior of this material when interacting with the human body must not have any toxic effects and must perform a specific task. For a material to be bioactive, it requires to be biocompatible and have a biological effect and provoke a positive and controlled biological response. Current biocompatible materials that are commonly used are gold, titanium, polymers, bioceramics, and composites [4–8].

Silicon was chosen as the material for this research due to its abundance and semiconductor abilities. Microfabricated silicon is widely used today in the microelectronics and photovoltaics industry [9, 10]. Silicon in its pure form is not biocompatible [11, 12]. However, silicon can be packaged in a biocompatible material such as titanium [13, 14]. It has been found that porous silicon is biocompatible [11]. The current method used for creating a porous layer is etching with hydrochloric acid. Acid etching is a long process that requires the use of dangerous chemicals and is consequently environmentally friendly. The challenge that silicon faces in the biomaterials industry is to find a superior surface alteration method.

1.2. Laser processing

Technology that easily controls and creates an accurate pattern on a microscale is required in the microelectronics industry. A good solution to this criterion is a laser, which has been commonly used for surface texturing of steel [15, 16]. It was found that this method of surface treatment allowed the generation of micropores with different characteristics. Unlike acid etching, a laser is great for the modification of silicon since it is very clean, high resolution, and controllability of intensity and depth of penetration. The Nd:YAG pulsed laser is a particularly good solution since it is cost-effective, stable, and has the required high power range. Another advantage to this method is that there are no chemicals involved, which eliminates the complex processes of preparation and environmental concerns. Above all, using a laser is a single-step process. The economic and simplistic benefits that are associated with this approach are valuable to the biomedical industry.

High-end picosecond and femtosecond pulsed laser systems have also been used for generation of porous silicon particles [17, 18]. In this research, it is found that a Nd:YAG nanosecond pulse laser can achieve the desired biocompatible silicon. The nanosecond laser is much more economical and commercially available than the faster pulse lasers. The nanosecond laser is also currently used in the medical industry for procedures such as eye and dental surgeries [19, 20].

2. Laser processing and surface characterization

Microfabrication with lasers is becoming increasingly popular in many industries including biomaterials [21]. Laser irradiation introduces surface irregularities and chemical changes to the silicon surface. The laser irradiates a simple line pattern onto pure silicon with <100> orientation. There are a number of methods used to analyze the condition of the laser-processed substrat. Images of the samples are taken with field emission scanning electron microscopy (FESEM) and 3D optical microscopy.

2.1. Laser system

The laser used in this research is a SOL-20 1064 nm Nd:YAG nanosecond laser by Bright Solutions Inc. The JD2204 Sino Galvo two-axis Galvo scanner has an input of 10 mm and a beam displacement of 13.4 mm. The theoretically determined spot size diameter is 19 μm. The laser pulses can range from lengths of 6 to 35 ns, frequencies of 10 to 100 kHz, powers up to 20 W, and scanning speeds up to 3000 mm/s. For this research, scanning speeds of 100–1000 mm/s, powers of 7, 10, and 15 W, and frequencies of 25, 70, and 100 kHz are used. Line spacing varies from 0.025, 0.05, and 0.10 mm. Overlap number, or number of times the laser repeats the same pattern, varies from 1, 2, and 3. The manipulation of these parameters is easily executed through the laser-operating software.

2.2. Biocompatibility evaluation

The biocompatibility of a material is influenced by surface roughness, reflectivity, and chemical content of the substrate. The chemical content is assessed using micro-Raman and energy-dispersive X-ray (EDX) analysis. The surface roughness is determined with the use of 3D optical microscopy, and the reflectivity is determined with light spectroscopy. The biocompatibility is also determined with the use of simulated body fluid, which is a form of *in vitro* assessment—testing done outside of the body. Simulated body fluid is a solution that mimics the ion concentration of human blood plasma. When a biocompatible material is submerged in the liquid, hydroxyapatite forms on the surface [22, 23]. The submerged samples in the SBF are kept in an incubator at 36.5°C for up to 6 weeks.

Cell interactions with the laser-processed silicon substrate are also evaluated with cultured mouse embryonic fibroblasts (NIH 3T3). Cells are seeded at 2400 cells/cm^2 in triplicate and incubated for 72 h at 37°C. The samples are incubated under 5% CO_2 in Dulbecco's modified Eagle medium (DMEM) supplemented with 10% heat-inactivated calf serum. Phosphate-buffered saline (PBS) was then used to rinse the nonadherent cells from the samples overnight at 4°C. Staining was then done to the samples with phalloidin (1:2000 dilution) and draq5 (1:10,000 dilution) overnight for fluorescence imaging.

2.3. Temperature evaluation

Different frequencies, powers, and pulse widths change the behavior of the laser pulses. Determining the temperature will help investigate the pulse energy and how it affects the

surface topographic properties and chemical structure. The surface temperature is modeled using the two-dimensional heat equation in cylindrical coordinates. The heat equation in cylindrical coordinates is found in Eq. (1).

$$\frac{1}{r}\frac{\partial}{\partial r}\left(\kappa r\frac{\partial T}{\partial r}\right) + \frac{1}{r^2}\frac{\partial}{\partial \phi}\left(\kappa\frac{\partial T}{\partial \phi}\right) + \frac{\partial}{\partial z}\left(\kappa\frac{\partial T}{\partial z}\right) + \dot{q} = \rho c_p\frac{\partial T}{\partial t} \tag{1}$$

where κ is the heat conduction coefficient, ρ is the material density (kg/m^3), c_p is the specific heat (J/kgK), and $\dot{q}$ is the rate at which energy is generated per unit volume of the medium (W/m^3) [24]. Since it is assumed that κ, ρ, and c_p are constant, and there is no energy generation within the silicon ($\dot{q} = 0$), Eq. (1) can be simplified into Eq. (2).

$$\frac{1}{r}\frac{\partial}{\partial r}\left(r\frac{\partial T}{\partial r}\right) + \frac{\partial}{\partial z}\left(\frac{\partial T}{\partial z}\right) = \frac{1}{a}\frac{\partial T}{\partial t} \tag{2}$$

where $a = \kappa/\rho c_p$, which is the thermal diffusivity (m^2/s). The boundary conditions for this equation include the initial temperature being room temperature, the pulse intensity is at its maximum during the pulse at $z = 0$, the intensity is zero between pulses, and the temperature change is zero at $r = \infty$, and $z = \infty$. With these conditions, the single-pulse temperature change of a high absorption material, ΔT, for a square pulse, can be obtained (Eq. (3)) [25].

$$\Delta T(r, z, \tau) = \frac{I_{max}\gamma\sqrt{\kappa}}{\sqrt{\pi}K}\int_0^\tau \frac{1}{\sqrt{t}\left[1 + \frac{8\kappa t}{W^2}\right]}e^{-\left[\frac{z^2}{4\kappa t} + \frac{r^2}{4\kappa t + \frac{1}{2}W^2}\right]}dt \tag{3}$$

$$\text{where } I_{max} = \frac{P_{peak}}{A} = \frac{4P_{measured}}{\pi d^2 f\tau} \tag{4}$$

where I_{max} (Eq. (4)) is the peak intensity which is the peak power divided by the spot area, $P_{measured}$ is the experimental measured power, f is the pulse frequency, τ is the pulse duration, γ is equal to the Fresnel energy reflectivity (R) subtracted from 1 (1–R) with a R value of 0.325 and a γ value of 0.675, κ is Silicon's diffusivity with a value of $9.07{\times}10^{-3}$ m^2/s, K is Silicon's conductivity with a value of 155 W/mK, τ is the laser pulse duration, W is the beam's filed radius (1/e) with a value of $1.94{\times}10^{-5}$ m, z is the ablation pit depth, and r is the ablation pit radius. Using this equation with the assumption that the pulse is square-shaped, the temperature can be determined at the center of ablation (r = 0) and at the surface (z = 0). From Eq. (3), an analytical expression can be made to determine the depth of the ablated groove at the center of the ablation with respect to radius by using the mean value theorem.

$$h(r) = \sqrt{-4\kappa\tau\ln\left\{\frac{\beta K\Delta T_B}{\gamma I_{max}}\sqrt{\frac{\pi}{\kappa\beta\tau}}\left(1 + \frac{8\beta\kappa\tau}{W^2}\right)\right\} - \frac{r^2}{1 + \frac{W^2}{8\beta\kappa\tau}}} \leq h(0) \tag{5}$$

where β is an experimentally determined correction factor of 0.5 and ΔT_B is silicon's boiling temperature of 2972 K. A more accurate representation of the experimental results found in

Eqs. (6) and (7) will determine the ablation depth after a train of pulses. Each consecutive pulse adds to the penetration of the preceding pulse, S, resulting in a deeper groove.

$$h_{scan}(r) = h(r) + h(S - r) \tag{6}$$

$$S = \frac{v\_scan}{f} \tag{7}$$

where S is the spatial separation between each consecutive pulse, v_scan is the scanning speed in m/s, and f is the pulse frequency.

3. Effect of scanning parameters

The three scanning parameters discussed in this section are overlap number, line spacing, and scanning speed. Each of these is easily set through the laser-operating software. These parameters have a direct effect of the surface topography and oxidation levels of the silicon substrates.

3.1. Topography analysis

The field emission scanning electron microscope images are an effective way of investigating the physical results from the laser ablation on the silicon samples. **Figure 1** shows the effect of different overlap numbers. At 1 overlap (OL), the line pattern is distinct and relatively clean. When the OL number is increased to 2, the line pattern is less definite and contains more irregularities. Finally, increasing the overlap number once again to 3, the line pattern is almost unrecognizable with a substantial amount of imperfections.

The effect of different line spacing was then investigated with FESEM. The overlap number was kept constant at 1. At the largest line spacing of 0.10 mm, the line pattern is discrete. At the smallest line spacing of 0.025 mm, the amount of imperfections is high with no distinctive line separation. The effect of line spacing can be seen in **Figure 2**.

Knowing that a higher overlap number and a smaller line spacing made for the highest level of laser-ablated substrate, a sample with 0.025 mm line spacing and three overlaps was created to observe the surface characteristics. The high magnification FESEM image in **Figure 3** of this sample shows a nanofibrous substrate. These nanofibers are the result of a high-energy reactive plume that forms on the surface during laser ablation [26]. The plume generates a heat-affected zone that causes the silicon ions to react with the oxygen ions, creating these nanoscale SiO_2 fibers [27–29].

The effect of scanning speed was then investigated with 3D optical microscopy. The data of the results from scanning speeds of 100, 200, 500, 800, and 1000 mm/s are mapped and compared in **Figure 4**. It is expected that the lower scanning speeds have larger depths due to a higher number of pulses ablating the surface area. However, with a closer look at **Figure 4**, the lower scanning speeds have shallow depths and a relatively high wall of built-up material along the
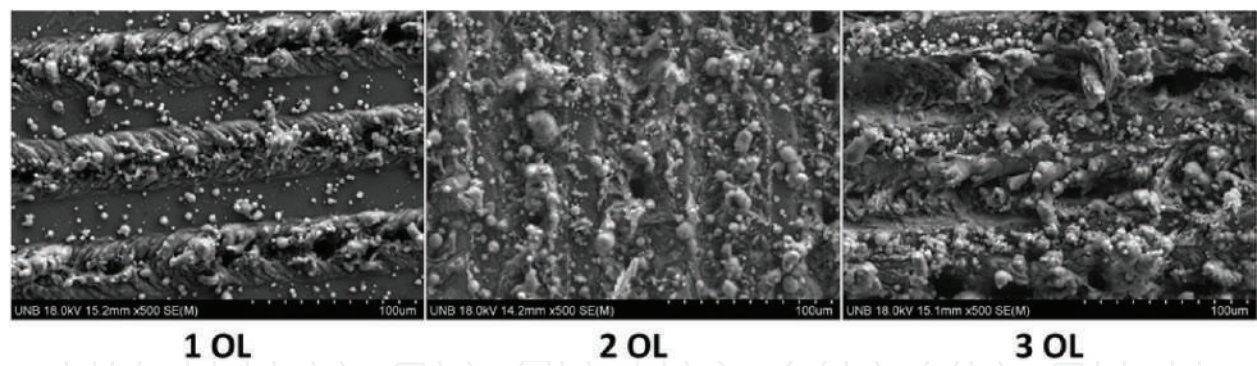
Figure 1. FESEM images of pattern overlaps of 1, 2, and 3 with a line spacing of 0.10 mm, a laser power of 10.5 W, a frequency of 100 kHz, and a scanning speed of 400 mm/s.
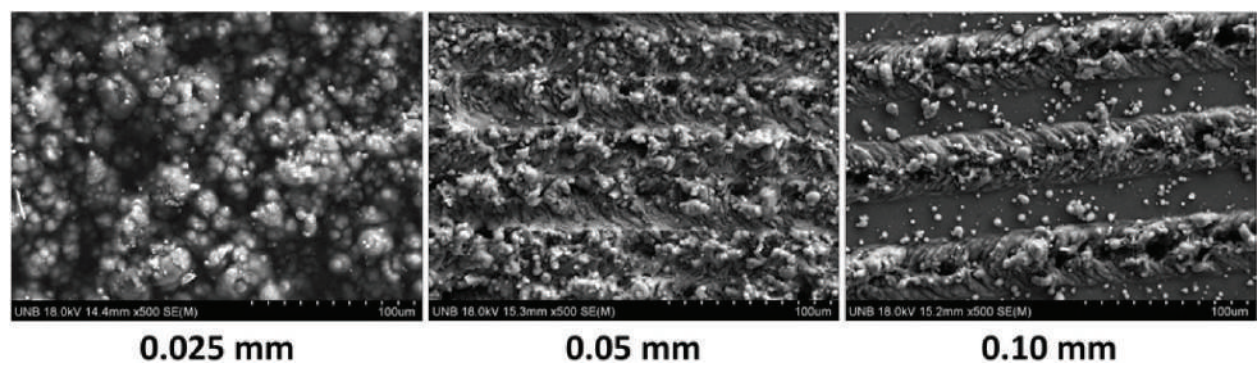

Figure 2. FESEM images of line spacing of 0.025, 0.05, and 0.10 mm with an overlap number of 1, a laser power of 13.3 W, a frequency of 100 kHz, and a scanning speed of 400 mm/s.
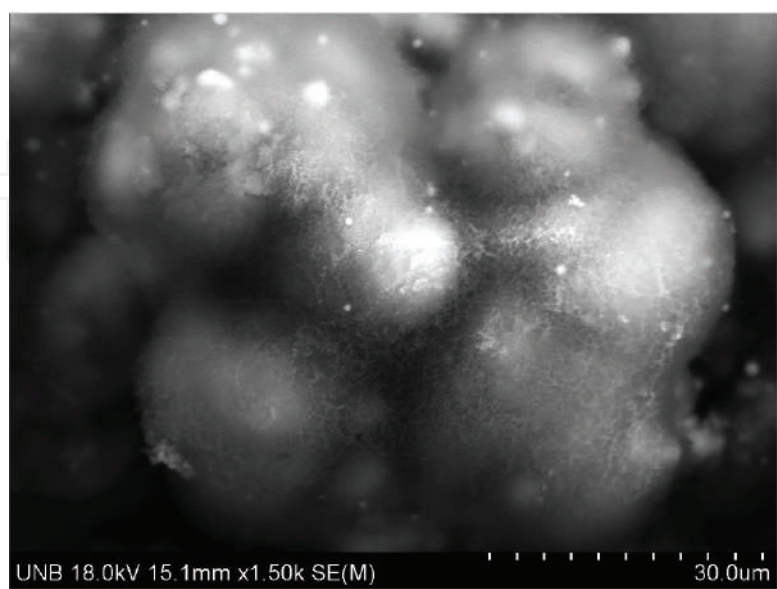

Figure 3. Presence of nanofibers detected on FESEM image of sample with three overlaps and 0.025 mm line spacing with power of 13.3 W, frequency of 100 kHz, and a scanning speed of 400 mm/s.
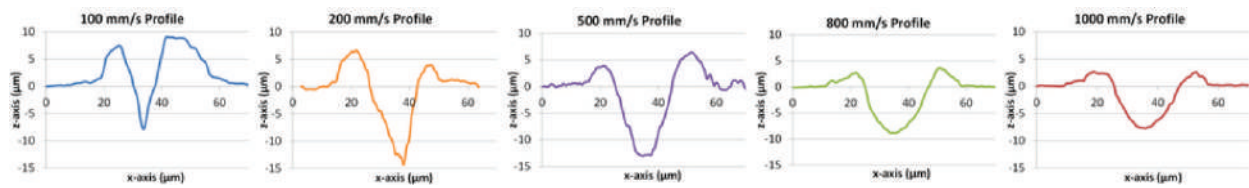
Figure 4. Profile data from the 3D optical microscope for scanning speeds of 100, 200, 500, 800, and 1000 mm/s at an overlap number of 1, a power of 15 W, and a frequency of 100 kHz.
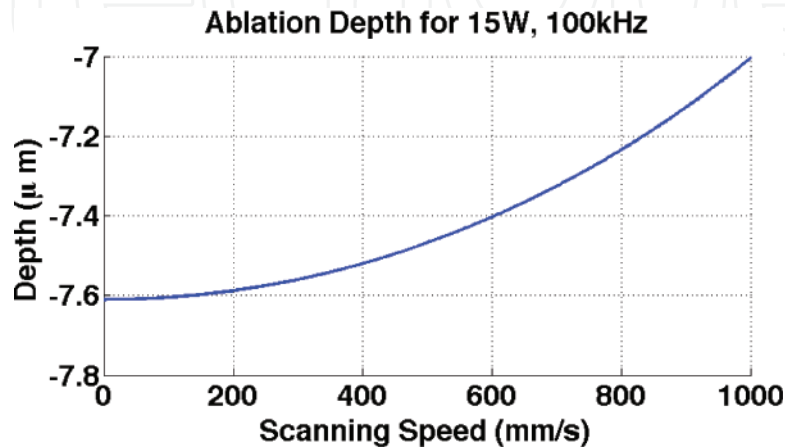

Figure 5. Ablation depth after a train of pulses at difference scanning speeds at a power of 15 W and a frequency of 100 kHz.

sides of the groove. At higher scanning speeds, when the pulses are farther apart, there is less penetration on the surface, leading to a shallower groove. At lower scanning speeds, the high-temperature ablated material from the walls caves back into the deep groove and solidifies into a much shallower groove than initially dredged. Scanning speeds of 200 and 800 mm/s show a deep groove with a smaller amount of material built up than the 100 mm/s sample.

Eqs. (6) and (7) are then used to find the theoretical ablation depths at various scanning speeds. Observing the trend in **Figure 5**, it is clear that the ablation depth decreases with increasing scanning speed. Both the experimental data and theoretical results are in close agreement.

3.2. Bioactivity assessment

Each sample was submerged in simulated body fluid (SBF) for 6 weeks and kept at a constant temperature of 36.5°C. The samples were then emerged from the fluid and assessed with energy-dispersive X-ray (EDX). The SBF-soaked samples were found to contain a traces of phosphorous and calcium, which is indicative of the presence of a bone-like apatite. Hydroxy-apatite is formed by the nucleation of calcium phosphate ions [5, 27]. The silicon oxide layer created by the laser plume has a negative charge, which attracts the positively charged calcium phosphate. The resulting substrate contains this bone-like apatite, which was seen on the laser-treated silicon samples. The EDX results from the sample with three overlap and 0.025 mm line spacing can be seen in **Figure 6**.
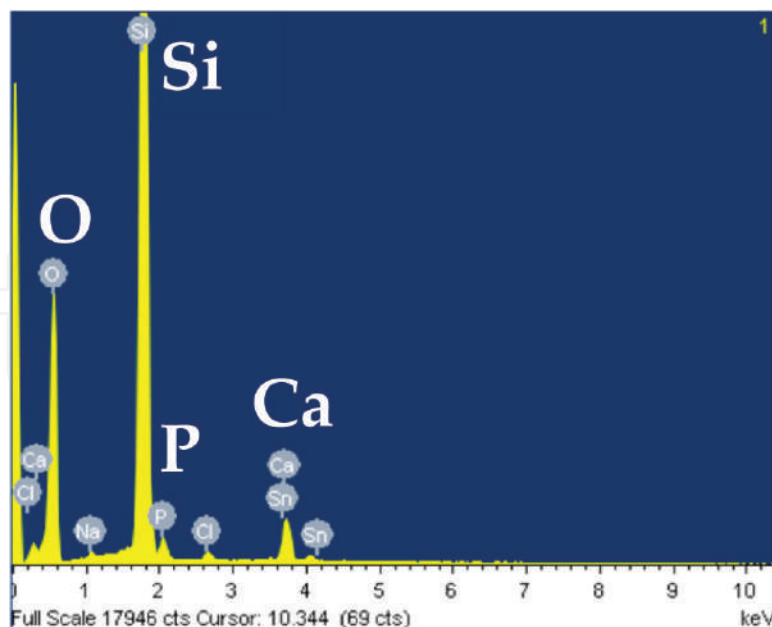
Figure 6. EDX results of sample with three overlaps, 0.025 mm line spacing, 400 mm/s, a power of 13.3 W, and a frequency of 400 mm/s.

This presence of bone-like apatite confirms that the biocompatibility of pure silicon was enhanced with nanosecond laser pulses. A smaller line spacing and higher overlap number generates more SiO_2 nanofibers, which provides a favorable site for the nucleation of apatite.

4. Effect of frequency

The range of frequencies used in this section is 25, 70, and 100 kHz. For these experiments, the scanning speed was kept constant at 100 mm/s, the power at 15W, and the overlap number at 1.

4.1. Topography analysis

Figures 7 and **8** show the topography changes in the frequency samples. A lower frequency produces a wider and shallower groove, while the higher frequencies yield a thinner yet deeper ablated groove. The theoretical results in for a single pulse in **Figure 9** show that the groove increases in depth and decreases in width as frequency increases, which is in close agreement with the experimental results.

4.2. Temperature analysis

The temperature is determined for each frequency with Eq. (3) and can be found in **Figure 10**. The higher temperatures are associated with the lower frequencies on both z-axis and r-axis. By increasing the frequency, the pulse energy decreases which results in lower temperatures and a smaller heat-affected zone [30]. Due to reduced size of the heat-affected zone, the shape of the groove consequently changes size as well. This results in the thinner grooves at higher
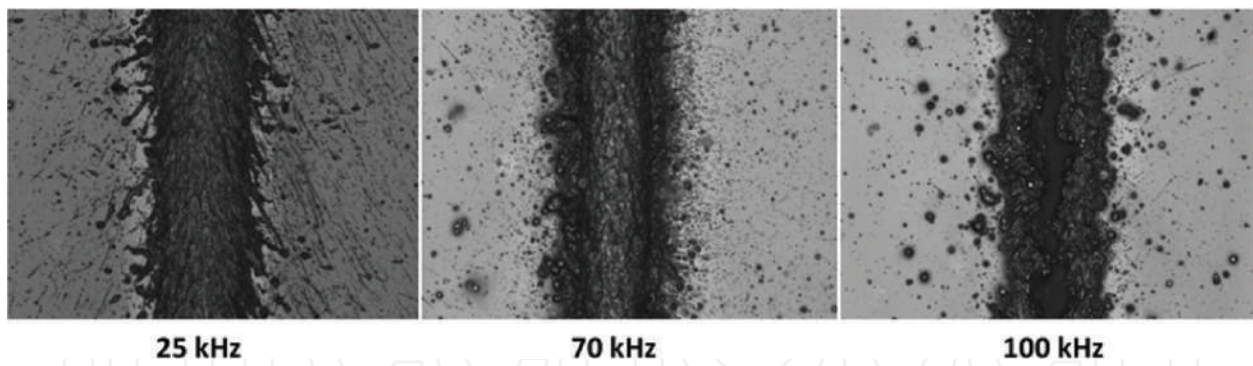
Figure 7. 3D optical microscopy images of samples with frequencies of 25, 70, and 100 kHz at a power of 15 W, a scanning speed of 100 mm/s, and 1 overlap.
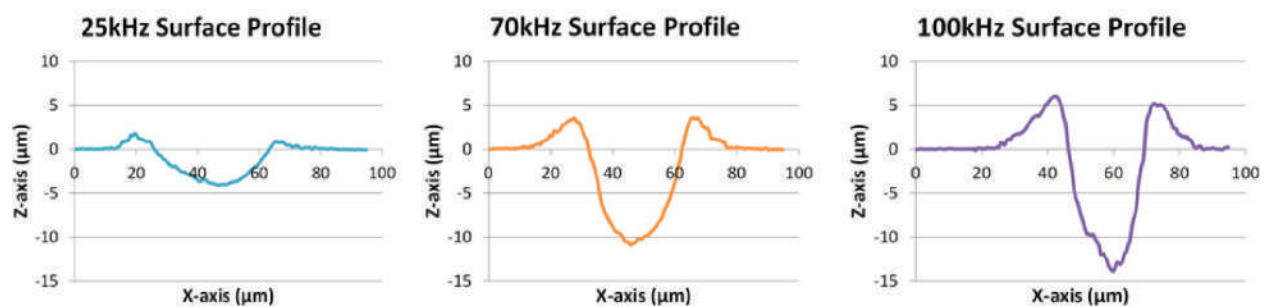

Figure 8. Experimental profile data from the 3D optical microscope for frequencies of 25, 70, and 100 kHz at an overlap number of 1, a power of 15 W, and a scanning speed of 100 mm/s.
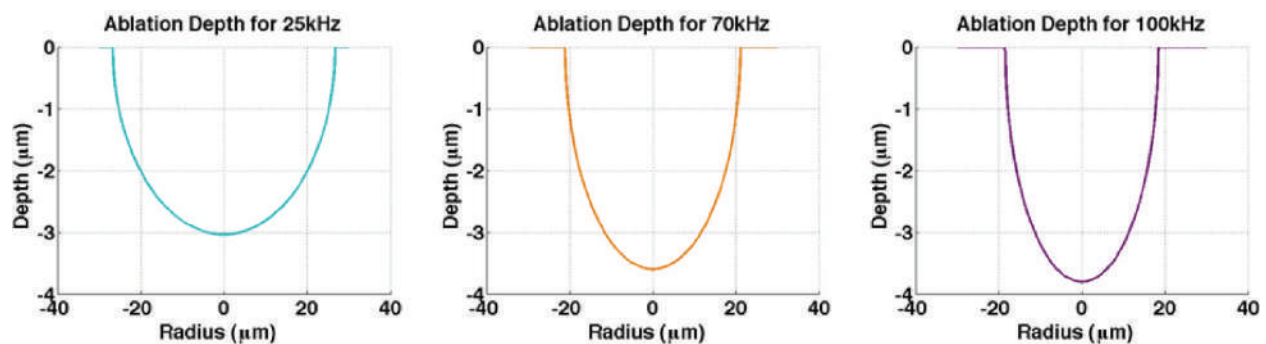

Figure 9. Theoretical profile data for a single pulse for frequencies of 25, 70, and 100 kHz at an overlap number of 1, a power of 15 W, and a scanning speed of 100 mm/s.

frequencies. Each recurring pulse adds to the penetration of preceding pulse. Higher frequencies have more pulses, resulting in a deeper penetration of the surface, which develops a trench with a larger depth.

4.3. Bioactivity assessment

Mouse embryonic fibroblast cell interactions were examined for each frequency. The cell count in **Figure 11** establishes that there are a higher number of cells in the higher frequency grooves.
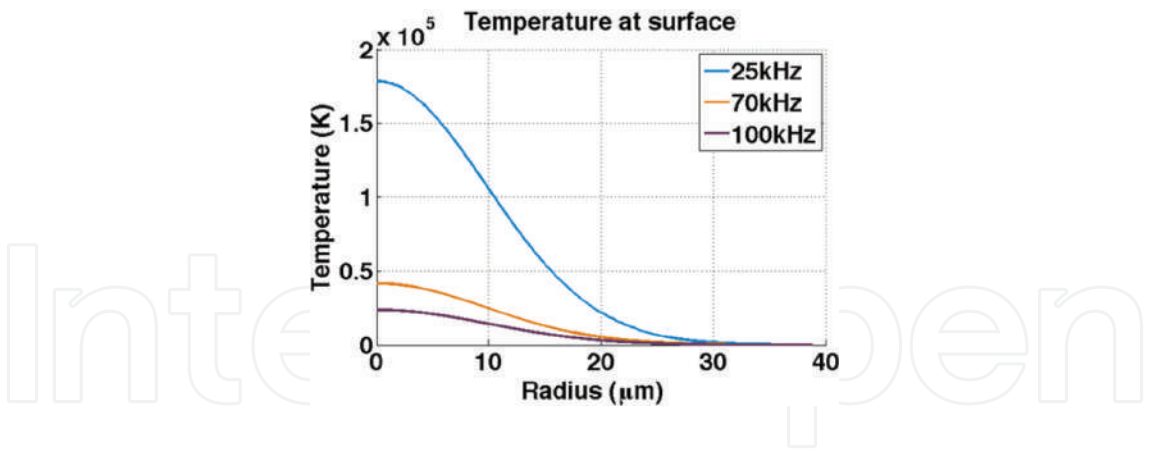
Figure 10. The single-pulse temperature on the surface of the silicon with respect to radius.
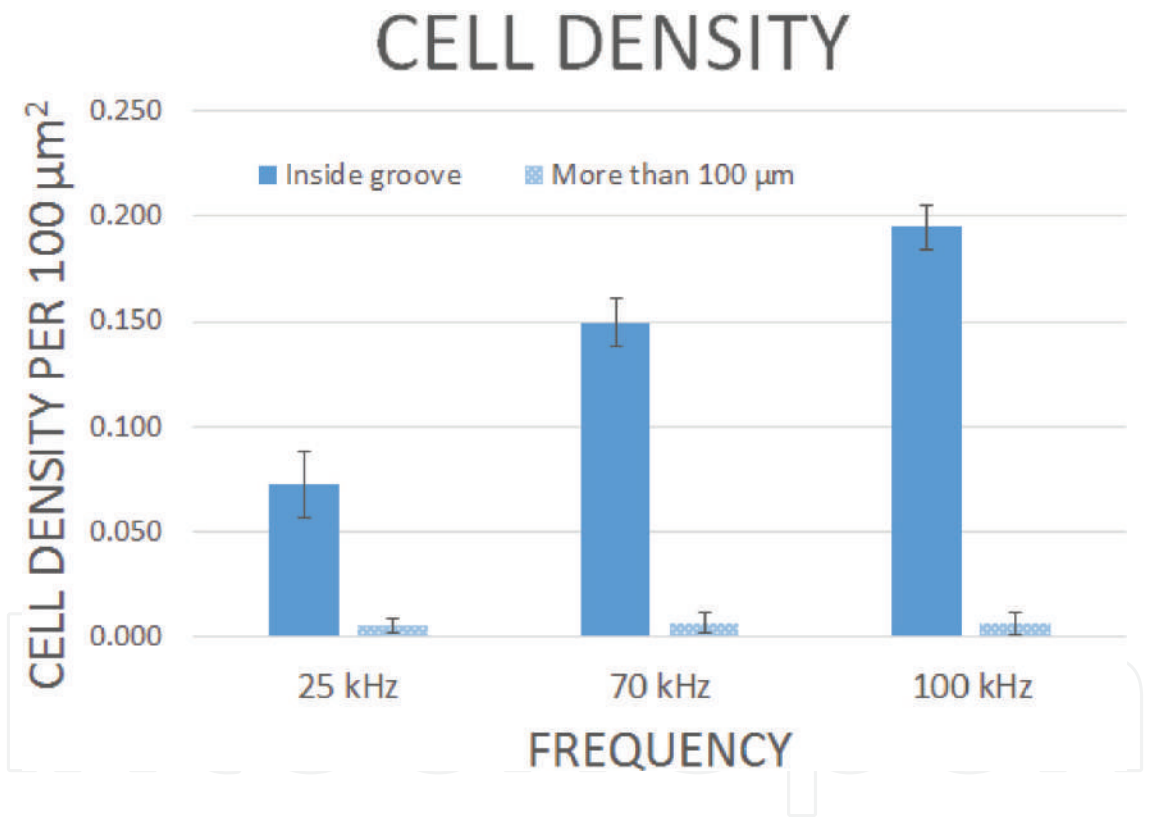
Figure 11. The number of cells within the laser-treated groove for each frequency as well as the amount of cells outside the groove within 100 μm from the edge of the groove [30].

The cells show a strong preference for the treated areas and show avoidance in the untreated areas. There is also a presence of fibronectin within the cells, which is an ECM protein secreted during embryonic development and wound healing, potentially leading to collagen deposition and tissue morphogenesis [30, 31]. These results confirm that the biocompatibility is enhanced with higher frequencies.

5. Effect of power

Laser power immensely influences the surface properties when treatment is done to a material. The power for this section varies from 7, 10 to 15 W. For these experiments, the frequency was kept constant at 100 kHz, the scanning speed was set to 400 mm/s, and the overlap number was 1.

5.1. Topography analysis

The FESEM images of each power sample are shown in **Figure 12**. The experimental 3D optical microscopy profile data is shown in **Figure 13**. These results show that at higher powers, the groove will increase in both width and depth. Unlike the frequency trends, the size of the heat-affected zone increases with power. The theoretical single-pulse depths found with Eq. (5) are shown in **Figure 14**. These results also show that the groove width and depth increase with power and are in close agreement with the experimental results.
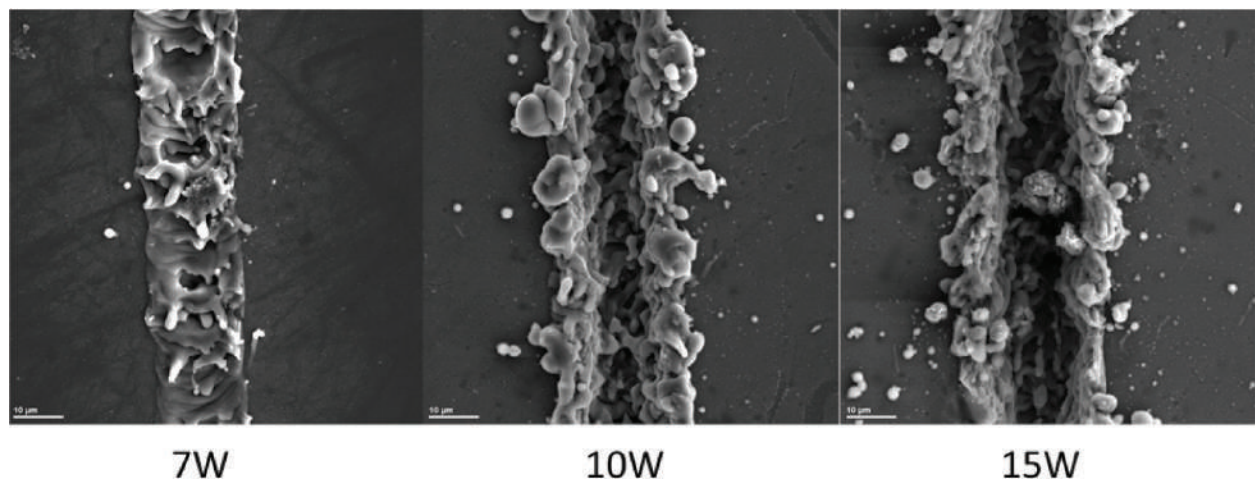

Figure 12. FESEM images of samples with powers of 7, 10, and 15 W at a frequency of 100 kHz, a scanning speed of 400 mm/s, and 1 overlap.
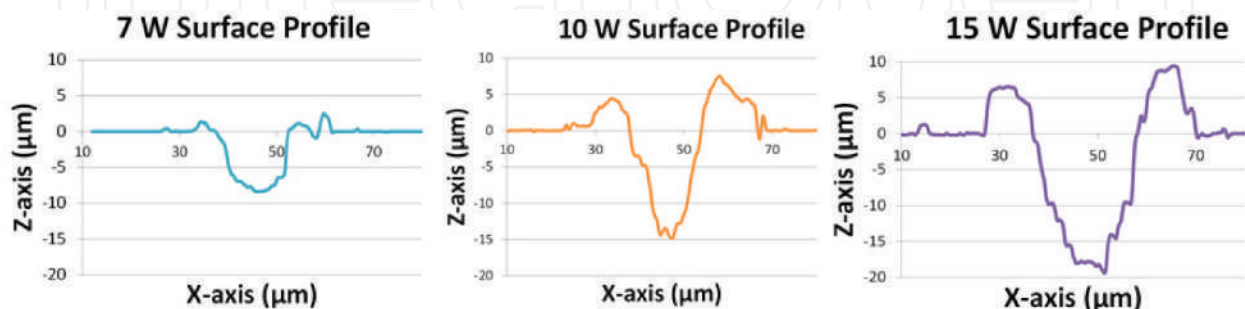

Figure 13. Experimental profile data from the 3D optical microscope for powers of 7, 10, and 15 W at an overlap number of 1, a frequency of 100 kHz, and a scanning speed of 400 mm/s.
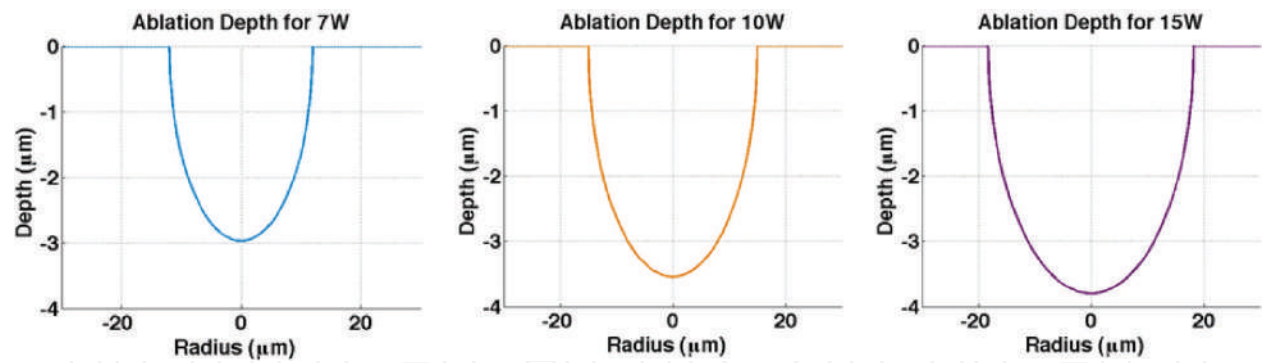
Figure 14. Theoretical profile data for a single pulse for powers of 7, 10, and 15 W with an overlap number of 1, a frequency of 100 kHz, and a scanning speed of 400 mm/s.

5.2. Temperature analysis

The temperature is determined for each power with Eq. (3) and can be found in **Figure 15**. As expected, the higher temperatures are found with higher powers. At lower powers, the heat-affected zone is smaller, allowing for both a thinner and shallower groove. When the pulse power is increased, the temperatures in the high-density plume are increased, causing more generation of the SiO_2 nanofibers [26].

5.3. Bioactivity assessment

Samples were once again assessed with fibroblast culturing for each power. When viewing the cell interactions under the microscope, cells were accumulated inside the laser-treated area as expected. Interestingly, the cell count was low directly beside the grooves and began to become more concentrated farther away from the edge of the groove. The fibroblasts avoided the zones immediately beside the grooves on each side. This can be seen in **Figure 16**.

This phenomenon is a result from the shockwave that is generated from the high-energy plume during laser ablation [26]. The shockwave transfers energy to the surface with results in high intensity thermal stress. The thermal shock causes a small zone directly beside the
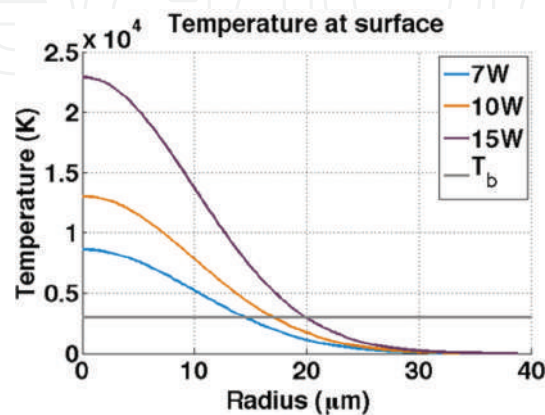

Figure 15. The single-pulse temperature on the surface of the silicon with respect to radius. T_b is the boiling temperature of silicon at 3538 K.
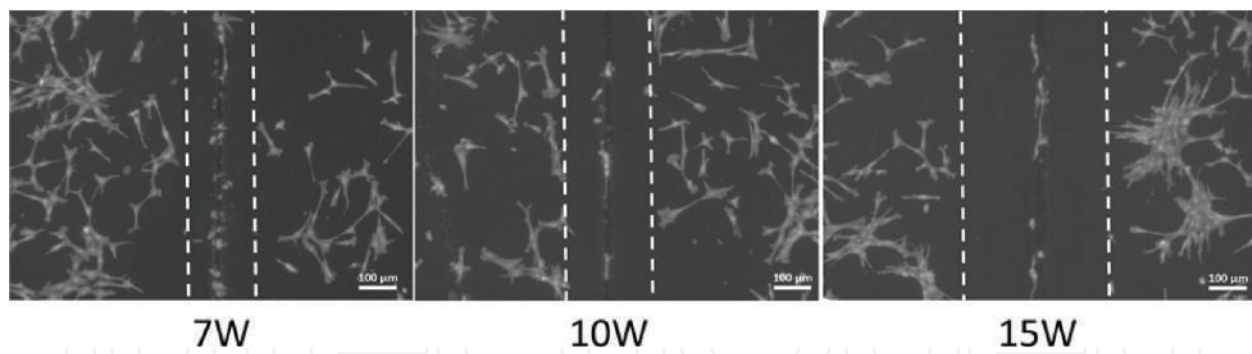
Figure 16. Fibroblast cells avoiding the zones beside the grooves for powers of 7, 10, and 15 W.

ablated areas, which contains residual stress. When the power is increased, there is a larger transfer energy, resulting in a larger stress zone. These residual stress zones contain mismatched crystal orientations due to tensile stresses causing crystal distortion.

Knowing that the power level of the laser pulse can control the residual stress zone size and cell behavior, this research can provide opportunities in cell manipulation and cell programming.

6. Summary

This chapter aims to introduce nanosecond laser processing for the enhancement of biocompatibility of pure silicon for various biomedical technologies. These results can contribute to the design of manufacturing processes of innovative biomedical devices to enhance the quality of living for a number of individuals. This research investigates the trends of various laser parameters including three scanning parameters (line spacing, overlap number, and scanning speed), pulse frequency, and laser power. Biocompatible *in vitro* assessment was conducted through the use of simulated body fluid (SBF) and cell culturing with NIH 3T3 fibroblasts. Samples with smaller line spacing and higher overlap numbers showed more generation of SiO_2 nanofibers, which were shown to be biocompatible under SBF assessment. Biocompatibility increased with frequency due to the SiO_2 being more prominent on high frequency samples and containing more fibroblast cell proliferation. Fibroblasts also showed preference to higher powers. However, the heat-affected zone immediately outside the ablated areas showed a mismatch of crystal orientations causing residual stress. These stress zones were avoided by cells, which led to promising results for the potential in cell programming and manipulation.

Author details

Candace Colpitts and Amirkianoosh Kiani*

*Address all correspondence to: a.kiani@unb.ca

Silicon Hall: Laser Micro/Nanofabrication Facility, Department of Mechanical Engineering, University of New Brunswick, NB, Canada

References

[1] Turner AP, Pickup JC. Diabetes mellitus: Biosensors for research and management. Biosensors. 1985;**1**(1):85-115

[2] Grayson AR, et al. A BioMEMS review: MEMS technology for physiologically integrated devices. Proceedings of the IEEE. 2004;**92**(1):6-21

[3] Copeland JG, et al. Cardiac replacement with a total artificial heart as a bridge to transplantation. The New England Journal of Medicine. 2004;**351**(9):859-867

[4] Li X, et al. The use of nanoscaled fibers or tubes to improve biocompatibility and bioactivity of biomedical materials. Journal of Nanomaterials. 2013;**2013**:14

[5] Radmanesh M, Kiani A. Effects of laser pulse numbers on surface biocompatibility of titanium for implant fabrication. Journal of Biomaterials and Nanobiotechnology. 2015;**6**:168

[6] Swetha M, et al. Biocomposites containing natural polymers and hydroxyapatite for bone tissue engineering. International Journal of Biological Macromolecules. 2010;**47**(1):1-4

[7] Yue Z, et al. Controlled delivery for neuro-bionic devices. Advanced Drug Delivery Reviews. 2013;**65**(4):559-569

[8] Vallet-Regí M, Colilla M, González B. Medical applications of organic–inorganic hybrid materials within the field of silica-based bioceramics. Chemical Society Reviews. 2011;**40**(2):596-607

[9] Green ML, et al. Ultrathin (<4 nm) SiO_2 and Si–O–N gate dielectric layers for silicon microelectronics: Understanding the processing, structure, and physical and electrical limits. The Journal of Applied Physics. 2001;**90**(5):2057-2121. DOI: http://dx.doi.org/10.1063/1.1385803

[10] Jeong S, et al. Hybrid silicon nanocone-polymer solar cells. Nano Letters. 2012;**12**(6):2971-2976. Available: http://dx.doi.org/10.1021/nl300713x. DOI: 10.1021/nl300713x

[11] Buckberry L, Baylis S. Porous silicon as a biomaterial. Materials World. 1999;**7**:213-215

[12] Shaoqiang C, et al. Hydroxyapatite coating on porous silicon substrate obtained by precipitation process. Applied Surface Science. 2004;**230**(1):418-424

[13] Mwenifumbo S, et al. Cell/surface interactions on laser micro-textured titanium-coated silicon surfaces. The Journal of Materials Science: Materials in Medicine. 2007;**18**(1):9-23

[14] Myllymaa S, et al. Adhesion, spreading and osteogenic differentiation of mesenchymal stem cells cultured on micropatterned amorphous diamond, titanium, tantalum and chromium coatings on silicon. Journal of Materials Science: Materials in Medicine. 2010;**21**:329-341

[15] Vilhena LM, et al. Surface texturing by pulsed Nd:YAG laser. Tribology International. 2009;**42**(10):1496-1504. DOI: dx.doi.org/10.1016/j.triboint.2009.06.003

[16] Radmanesh M, Kiani A. Nd: YAG laser pulses ablation threshold of stainless steel 304. Materials Sciences and Applications. 2015;**6**(07):634

[17] Bonse J, et al. Femtosecond laser ablation of silicon–modification thresholds and morphology. Applied Physics A. 2002;**74**(1):19-25

[18] Kiani A, et al. Leaf-like nanotips synthesized on femtosecond laser-irradiated dielectric material. The Journal of Applied Physics. 2015;**117**(7):074306

[19] Wood JP, et al. Nanosecond pulse lasers for retinal applications. Lasers in Surgery and Medicine.2011;**43**(6):499-510

[20] Al-Hadeethi Y, et al. Data fitting to study ablated hard dental tissues by nanosecond laser irradiation. PLoS One. 2016;**11**(5):e0156093

[21] Khademhosseini A, et al. Microscale technologies for tissue engineering and biology. Proceedings of the National Academy of Sciences of the United States of America. 2006;**103**(8):2480-2487. DOI: 0507681102 [pii]

[22] Canham LT. Bioactive silicon structure fabrication through nanoetching techniques. Advanced Materials. 1995;**7**(12):1033-1037

[23] Kamitakahara M, et al. Bioactivity and mechanical properties of polydimethylsiloxane (PDMS)-CaO-SiO$_2$ hybrids with different PDMS contents. The Journal of Sol-Gel Science and Technology. 2001;**21**(1-2):75-81

[24] Incropera FP, et al. Introduction to convection. In: Anonymous, editors. Introduction to Heat Transfer. 5th ed. Danvers, MA, USA: John Wiley & Sons; 2007. pp. 57

[25] Hendow ST, Shakir SA. Structuring materials with nanosecond laser pulses. Optics Express. 2010;**18**(10):10188-10199

[26] Tavangar A, Tan B, Venkatakrishnan K. Study of the formation of 3-D titania nanofibrous structure by MHz femtosecond laser in ambient air. The Journal of Applied Physics. 2013;**113**(2):023102

[27] Tavangar A, Tan B, Venkatakrishnan K. The influence of laser-induced 3-D titania nanofibrous platforms on cell behavior. Journal of biomedical nanotechnology. 2013;**9**(11):1837-1846

[28] Kiani A, Venkatakrishnan K, Tan B. Optical absorption enhancement in 3D nanofibers coated on polymer substrate for photovoltaic devices. Optics Express. 2015;**23**(11):A569-A575

[29] Colpitts C, Kiani A. Synthesis of bioactive three-dimensional silicon-oxide nanofibrous structures on the silicon substrate for bionic devices' fabrication. Nanotechnology and Nanomaterials. 2016;**6**:1-7

[30] Colpitts C, et al. Mammalian fibroblast cells show strong preference for laser-generated hybrid amorphous silicon-SiO$_2$ textures. Journal of Applied Biomaterials and Functional Materials. 2016. DOI: D2673E51-9D76-4504-A673-13AAC5CE7AD3 [pii]

[31] Vega ME, Schwarzbauer JE. Collaboration of fibronectin matrix with other extracellular signals in morphogenesis and differentiation. Current Opinion in Cell Biology. 2016;**42**:1-6. DOI: S0955-0674(16)30055-2 [pii]

We are IntechOpen,
the world's leading publisher of
Open Access books
Built by scientists, for scientists

6,300
Open access books available

171,000
International authors and editors

190M
Downloads

Our authors are among the

154
Countries delivered to

TOP 1%
most cited scientists

12.2%
Contributors from top 500 universities

BOOK CITATION INDEX
CLARIVATE ANALYTICS
INDEXED

WEB OF SCIENCE™

Selection of our books indexed in the Book Citation Index
in Web of Science™ Core Collection (BKCI)

Interested in publishing with us?
Contact book.department@intechopen.com

Numbers displayed above are based on latest data collected.
For more information visit www.intechopen.com

Measurement and Simulation of Permeation and Diffusion in Native and Cultivated Tissue Constructs

Hao-Hsiang Hsu, Katharina Schimek, Uwe Marx and Ralf Pörtner

Additional information is available at the end of the chapter

Abstract

Characterization of native skin or cultured 3D skin models with respect to permeability plays an important role for the development and testing of pharmaceuticals and cosmetics. Extensive efforts have been dedicated to determining the key parameters describing permeability and diffusion. Whereas respective methods are well established for native skin biopsies, only few are available for 3D skin models, as these have usually much lower dimensions. In this chapter, some fundamentals about permeation and diffusion as well as state of the art of measurement methods used for skin biopsies are summarized. An alternative method for the determination of the permeation in a membrane insert system and the use of a modular simulation to support permeability studies is presented and discussed.

Keywords: skin models, permeation, diffusion, membrane insert system

1. Introduction

Permeability studies are indispensable to characterize the transport of substances through the skin, either natural skin or cultivated 3D skin models. This is evident for dermal drug delivery systems, where drugs can be applied in the form of creams or patches on the skin. Furthermore, permeability studies play an important role in toxicity tests applied in drug development as well as substance testing. In this respect, human three-dimensional skin models have become an interesting tool.

Animal experiments are still a common method of testing drugs and also for skin, which is ethically controversial, cost-intensive and time-consuming. The fact is that drug testing on

INTECH
open science | open minds

human skin is more efficient in comparison to animal skin just like rat, mouse and guinea pig [1, 2]. Furthermore, in 2013 the European Regulation (EC) No 1223/2009 entered into force, which prohibits animal experiments for cosmetics products. Artificial skin models based on human cells are intended to replace animal experiments. Especially the barrier function between artificial and human skin can differ, so permeation and diffusion investigation in this area is necessary.

Most methods for determination of diffusion and permeability parameters have been developed for large biopsies and can hardly be applied for small-scale 3D skin tissue cultures. But this is indispensable, if multi-well test systems with several samples run in parallel or multi-organ-chips are applied. Therefore, this chapter will first give a brief overview of standard methods used to investigate permeation and diffusion on the skin. Then an alternative method based on skin tissue cultures in a membrane insert system is introduced. By this, the permeation coefficient of substances through a skin-tissue barrier can be determined. The diffusion coefficient is estimated via parameter optimization performed in COMSOL Multiphysics. This software tool helps to describe the physical effects of the experimental set-ups more precisely and can further be used to reduce the required amount of experiments significantly.

2. Penetration, diffusion and permeation through the skin

Penetration describes the entering of a substance into the skin. The entering process and depth of substance penetration through the skin depends on the physical and chemical character of the substance and the skin. The permeation of the skin is the pathway of a substance from the surface to the blood vessel. From a scientific point of view, it is the permeation of a substance through the skin layers. Diffusion is the physical process of randomized particle movement. If a concentration gradient exists, the particles move in the direction of lower concentration.

The human skin consists of three layers, the epidermis, dermis and subcutis. The stratum corneum (horny layer) is the upper layer of the epidermis and forms the main barrier of the skin. Substances such as drugs and chemicals penetrate through the skin barrier in three possible routes: the transcellular, the intercellular and the appendageal route (see **Figure 1**) [3–5].

The transcellular route leads the permeating substances directly through the cells. Here, the substances have to pass alternating lipophilic and hydrophilic layers. This is probably the
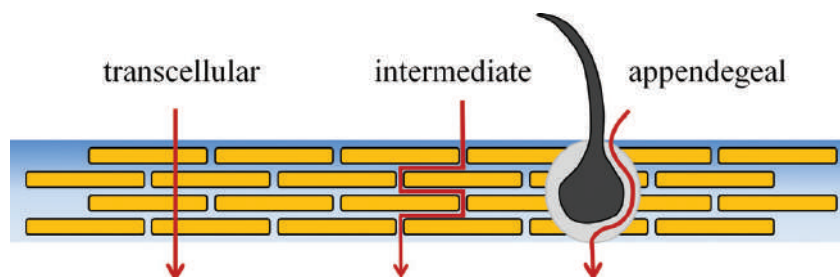

Figure 1. Schematic illustration of the three possible pathways of a permeating substance through the stratum corneum.

most difficult way for substances, because they should have lipophilic and hydrophilic properties. Until now, it is not clear if hydrophilic substances choose this pathway [6].

Alternatively, there is a way through the intercellular spaces between the cells. This is called the intercellular route. The intermediate space consists of cholesterols, ceramides and free fatty acids [7]. Because of the fatty acids, lipophilic substances can pass easier through the intercellular route in contrast to lipophobic substances [8]. Another barrier in this intercellular space is the tight junctions [9]. These are networks of strands which are formed by membrane proteins connecting cells. They are located between the keratinocytes in the stratum granulosum of the epidermis. An important function of the tight junctions, which are formed during the differentiation of keratinocytes, is to protect the skin from water loss [10].

The appendageal route describes the penetration of a substance through skin appendages like hair follicles and glands. Since hair follicles and glands build only a small part of the human skin, their relevance for skin permeation was neglected for a long time. Its importance was shown recently by a researcher as permeation is better in a skin area containing hair follicles and glands in comparison to an area without them. A specific characteristic of the hair follicle is it reservoir function. In follicles, substances can be stored up to 10 days and can penetrate gradually into the skin. This aspect is interesting for drug delivery over the skin. For example, alcohol prefers the appendageal penetration route, as it would otherwise evaporate quite fast on the surface of the skin. [11–14]

So far the penetration and permeation in the skin was described. To get more in detail, the physical aspect of diffusion and permeation will be explained. Diffusion is a transport process where molecules move via Brownian motion in a volume or area. It is driven by the concentration gradient in the direction from higher to lower concentration [15]. Adolf Fick (1829–1901) verified the coherence between heat transfer and diffusion, which led to the Fick's first law of diffusion:

$$F = -D \frac{\partial C}{\partial x} \tag{1}$$

According to Eq. (1), the flux F in the one partial direction x is proportional to the gradient of concentration C. D is the diffusion coefficient or diffusivity. [16, 17]

Permeation is an aspect of diffusion. Whereas diffusion is related to the movement of molecules in a system, permeation describes how fast molecules move through a system. An example is the permeation of a substance within a volume V_A and a donor concentration c_D through a membrane with a surface A. The acceptor concentration c_A of the permeating substance on the other side can be detected over the time t. Eq. (2) for the permeation coefficient P can be derived from the Fick's law of diffusion [18, 19]:

$$\frac{dc_A}{dt} = P \cdot A \frac{c_D}{V_A} \tag{2}$$

This equation can only be used for $c_D \gg c_A$. With respect to skin, the permeation coefficient is the preferred parameter, as it is easier to measure compared to the diffusion coefficient. Due to the different layers of the skin, permeation and diffusion coefficient changes all the time from layer to layer.

3. State of the art for investigation of penetration, diffusion and permeation within the skin

To understand and investigate diffusion and permeation of the skin biopsies, several methods have been established. Some are summarized in the following.

The Franz diffusion cell is a well-known device to measure the permeation of a substance through a skin biopsy. This device consists of two chambers where the skin biopsy (or any other barrier) is fixed in between. The test substance can be applied to the top chamber (donor) of the skin; it permeates through the barrier into the bottom chamber (acceptor). The fluid in the bottom chamber is mixed by means of a magnetic stirrer. On this side, samples can be taken and the concentration can be analyzed. The concentration of the acceptor is plotted over the time and the permeation coefficient can be calculated according to Eq. (2). The whole system can be temperature-controlled. The usual size (height) of a Franz diffusion cell is in the range of 19–179 mm. Besides permeation investigation, this system is also used to test the quality of skin models and the effects of pharmaceutical substances on the skin. [18, 20–26]

Fluorescence recovery after photobleaching (FRAP) is a method to measure molecular diffusion in tissues or gels, mainly for high molecular weight compounds. For this, the substance to be analyzed must be labeled with a fluorochrome. Mostly fluorescence-labeled proteins or FITC-dextranes (fluorescein isothiocyanate-dextranes) with different molecular sizes are used. The tissues or gels have to be soaked with this substance. This can be realized by storing the material in the fluorescence substance for some days or in case of a gel, to directly polymerize in the fluorescent substance. Then, a confocal laser is used to bleach out a certain area (mostly a line or a point) in the material. Because of diffusion, bleached molecules will move and change their position with fluorescent particles and the fluorescence recovers. After the bleaching process, the area will be scanned several times. The recovery time of fluorescence intensity is used to determine the diffusion coefficient of the substance in the material. For this, software for image analysis is used. [27–30]

Further examples for imaging methods for the determination of diffusion of molecules in skin are Fourier-transform-infrared (FTIR) spectroscopy [31, 32], two-photon fluorescence correlation spectroscopy in combination with fluorescence correlation spectroscopy (FCS) [33, 34] and optical coherence tomography [35]. These methods are noninvasive and nondestructive. Furthermore, some of them can detect molecules without fluorescence labeling. One big disadvantage is the equipment. For these imaging methods, special microscopes or also cost-intensive tomographs are needed.

A method to investigate the penetration process of substances into the skin is tape stripping. After treatment of the skin with the substance of interest the stratum corneum is ripped of layer by layer with an adhesive film. Then, the amount of the substance can be analyzed. For this, there are different methods to determine the concentration of the substance. One method is to detect the substances directly on the film, for example titanium dioxide can be analyzed with X-ray fluorescent measurement and fluorescent-labeled substances can be detected via laser scanning microscopy. Another possibility is to remove the skin layer from the film and apply standardized analytical methods to determine the substance concentration. With tape stripping it is possible to observe where the substance of interest is localized and how deep

they can penetrate into the skin. It is minimal invasive and possible to investigate the penetration directly on human skin. A disadvantage of this method is the undefined thicknesses of the stripped layer. It varies from experiment to experiment and differs with the skin model or skin type. The thickness can be estimated by weighing. [36–39]

As mentioned before, the above methods all together provide a detailed characterization of diffusion and permeation effects within the skin. But most of them can hardly be adapted to skin tissue models used in drug and substance testing. Here usually small culture devices, e.g. 12- or 96-well plates are preferred, as they allow for handling of a large number of samples in parallel. Furthermore, most methods require treatment of the sample in one or the other way. Therefore, it is quite difficult to determine the time-depending changes of diffusion and permeation.

4. Skin tissue models

The need to evaluate skin permeation, test cosmetic products and toxicologically screen topically applied compounds is evident. Historically, several millions of animal experiments have been performed worldwide to address this purpose [40]. Since animal experiments are under massive debate, ethical and regulatory issues, but also severe differences between animal and human data pushed the development and commercialization of diverse *in vitro* skin models [41, 42]. Human skin equivalents (HSEs) can be categorized into two main groups: the epidermis-only and full-thickness models. For both, the differentiation of keratinocytes and hence development of the various layers of the epidermis is important to model actual skin barrier properties more closely. In this context, the direct exposure to air as well as the culture media that supply nutrients for cell growth and differentiation from below has been found to be beneficial [43]. Growing cells on a porous membrane is one of the most commonly used ways to accomplish this air-liquid interface culture. According to the Organization for Economic Co-operation and Development (OECD) test guideline 431 (skin corrosion) and 439 (skin irritation), currently validated skin models include EpiSkin™ (L'oreal, France), EpiDerm™ SIT (MatTek Corporation, USA), SkinEthic™ RHE (SkinEthic laboratories, France), EpiCS® (CellSystems, Germany) and LabCyte EPI-MODEL24 SIT (Japan Tissue Engineering Co., Japan). These 3D skin models are all composed of one cell type only, the keratinocytes, mimicking the epidermis of native human skin and are especially advantageous with respect to high reproducibility [44]. However still not validated, there are also commercially available full thickness skin models composed of an additional dermal layer (e.g., GraftSkin®, EpiDermFT®, and Pheninon®). The models described are nowadays widely used for animal-free tests in drug development as well as, the chemical and cosmetics industries.

5. Determination of permeation and diffusion coefficients in membrane insert systems via measurement and simulation

A common method for *in vitro* cultivation of skin models is the use of a membrane insert system. This system consists of a plastic vessel with a permeable membrane at the bottom. It enables the cultivation of skin tissue models in airlift on the membrane and guarantees the

supply of nutrients from below. As the membrane insert system has two separate chambers, it can be used for permeation studies similar to the Franz diffusion cell. In the following, an experimental procedure for the determination of permeation coefficients in Transwell® systems (12 and 96 well) and simulations with COMSOL Multiphysics for estimation of diffusion coefficients will be discussed. Details can be found in [53].

5.1. Measurement and simulation.

The scheme of a permeation experiment in a membrane insert system is shown in **Figure 2**. The tissue barrier is established on the membrane. It is composed of agarose gel or 3D tissue to validate the method. The 3D tissues consist of a collagen matrix with human fibroblasts within and HaCaT cells on the top of the matrix. On top of the barrier, the donor is applied. The donor contains the substance to be analyzed, which permeates through the barrier. The acceptor, which collects the permeating substance, is located on the other side of the membrane in the receiver vessel. Temperature, humidity and mixing are parameters that influence the permeation and should be kept constant. It is recommended to perform the experiment on a shaker in an incubator with 37°C and ≥90% humidity (conditions for human cell culture). To avoid hydrodynamic pressure, the fluid surface in the insert (donor) and in the receiver vessel (acceptor) should be on the same level. The used volume for the experiment in 12 and 96 Transwell® systems is shown in **Table 1**. Sampling, like in the Franz diffusion cell, is difficult because of the small volume in the acceptor. A solution is the use of fluorescence-labeled substances, by which the permeate concentration can be detected via fluorescence measurement in the receiver vessel. A more elaborate possibility is to run several permeation experiments in parallel and take a sample from one vessel per time point. Then, the concentration of the substance can be measured analytically.

The permeation experiment was simulated with COMSOL Multiphysics. This program is based on the finite element method and offers different physic simulation modules. This
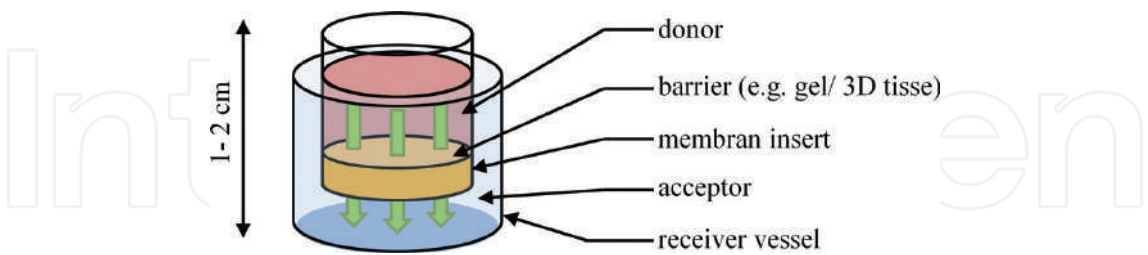
Figure 2. Schematic sketch of a membrane insert system.

Transwell System	Volume in acceptor	Volume in donor
96	75 µl	300 µl
12	590 µl	1845 µl

Table 1. Liquid volume in the acceptor and the donor in different membrane insert systems with a barrier of 2 mm thickness.

structure enables the computation of different physical problems in one simulation. The permeation experiment was simulated with the module "transport diluted species", which uses the Fick's law to simulate diffusion processes. In order to determine the diffusion coefficient, a parameter optimization was performed with the "optimization module". Some simplifications have to be done in order to simulate the experiment. In the experiment, the permeating substance passes through a barrier and a membrane. For the simulation, these two phases were resumed as one homogenous material. It is not possible to resolve the different phases, as investigations that are more detailed would be necessary. The diffusion coefficient of the permeating substance in the liquid phases (in donor and acceptor) was determined in preliminary mixing tests and was found to be 1×10^{-9} m^2/s. This parameter represents the molecular distribution in the mixing process. Furthermore, the geometry of the membrane insert system was simplified. In reality, the system is slightly conical. The simplified geometry is a cylinder. All boundaries of the geometry were set as "no slip". The concave surface of the agarose gel was approximated with a spherical shape. In **Figure 3**, the geometry and the mesh of the 96- and 12-well Transwell® systems are shown.

5.2. Influence of different settings and validation of the system.

Different membrane insert sizes influence the permeation within the system. Investigations with fluorescein sodium salt and 2% agarose gel in 96- and 12-well membrane insert systems are shown in **Figure 4a**. The time course of the acceptor concentration in the 12-well system was steeper in comparison to the 96-well system. Therefore, the fluorescein sodium salt permeates faster through the barrier in the 12-well system compared to the 96-well system. A reason for this is the concentration gradient in the gap between the membrane and the bottom of the receiver vessel. Because of the ratio "volume to permeation surface" and the gap size, the concentration will be balanced faster in case of the 12-well system. The gradient can be reduced by increasing the mixing frequency and amplitude. However, this is limited due to spillover of the liquid. By simulating these experiments, the different concentration distributions below the membrane can be visualized. In **Figure 4c** and **d** the concentration at different time points is plotted over the length below the membrane from the middle point to the edge of the receiver vessel (see red line on **Figure 4b**). The concentration difference between the middle and edge in 12-well systems is higher than that in 96-well systems. This indicates a better and faster concentration balance in the larger system, which explains the accelerated permeation.

The reproducibility of the suggested method is an important aspect. The permeation coefficient determined in different permeation experiments with fluorescein sodium salt through 2% agarose gel differed up to 40.9%. Although the value seems to be quite high, it is still within the range of deviation of permeability experiments with Franz diffusion cells reported in the literature [24]. It was found that small concentration variations during the preparation of the donor substance can cause large variation. By using one stock solution for different experiments, the deviation can be reduced to 29%. Further reasons for the deviation can also be small pipetting errors and variations of the barrier, for example, variation of the gel concentration or volume.
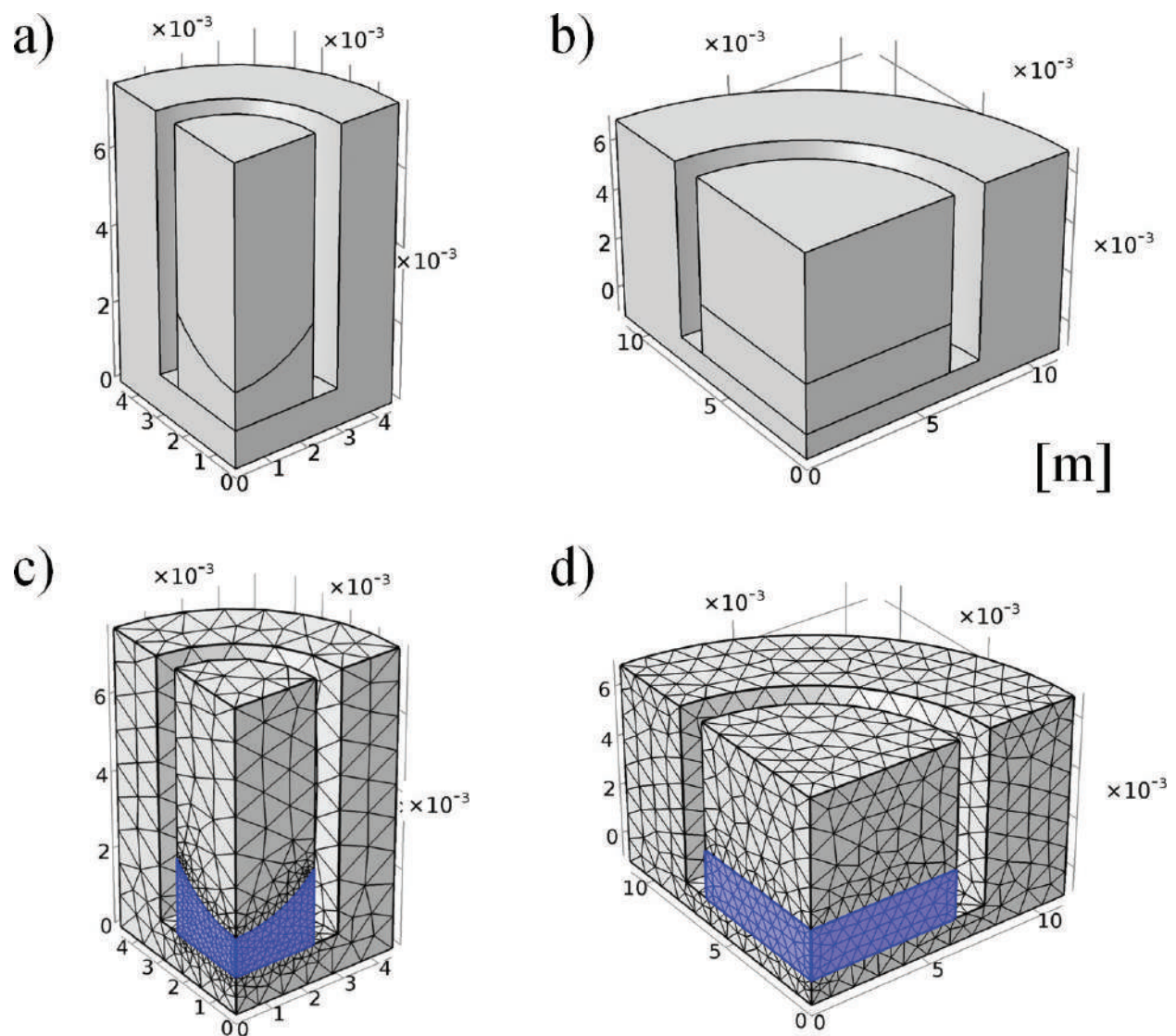
Figure 3. Geometry of the 96 a) and 12 b) Transwell® system and the used mesh c) and d) implemented in COMSOL **Multiphysics**.

The membrane itself also has an influence on the permeation. Same experiments as described above were carried out with different membranes in a 12 Transwell® system. Membranes consisting of polycarbonate (PC) with 0.4 and 3.0 µm pore size showed a quite similar permeation coefficient of 8.03 and 8.1×10^{-8} m/s. For polyethylene (PE) membranes with 0.4 µm pore size the mean value of the permeation coefficient was 5.94×10^{-8} m/s and for PE with 3.0 µm pore size it was 8.59×10^{-8} m/s (see **Figure 6a**). Except for the PE membrane with pore size of 3.0 µm there is no significant difference. The reason for this is the pore density of the membrane. In total, the pore surface of PE membranes with 0.4 µm pore size is 0.25 mm² per 1 cm² and for the other membranes 6.3–7.05 mm² per 1 cm². The material of the membrane seems not to influence the permeation.

The suggested method is sensitive enough to determine a cover layer of HaCaT cells of 3D skin tissue. To prove this, in a permeation experiment different 3D tissue model was tested in
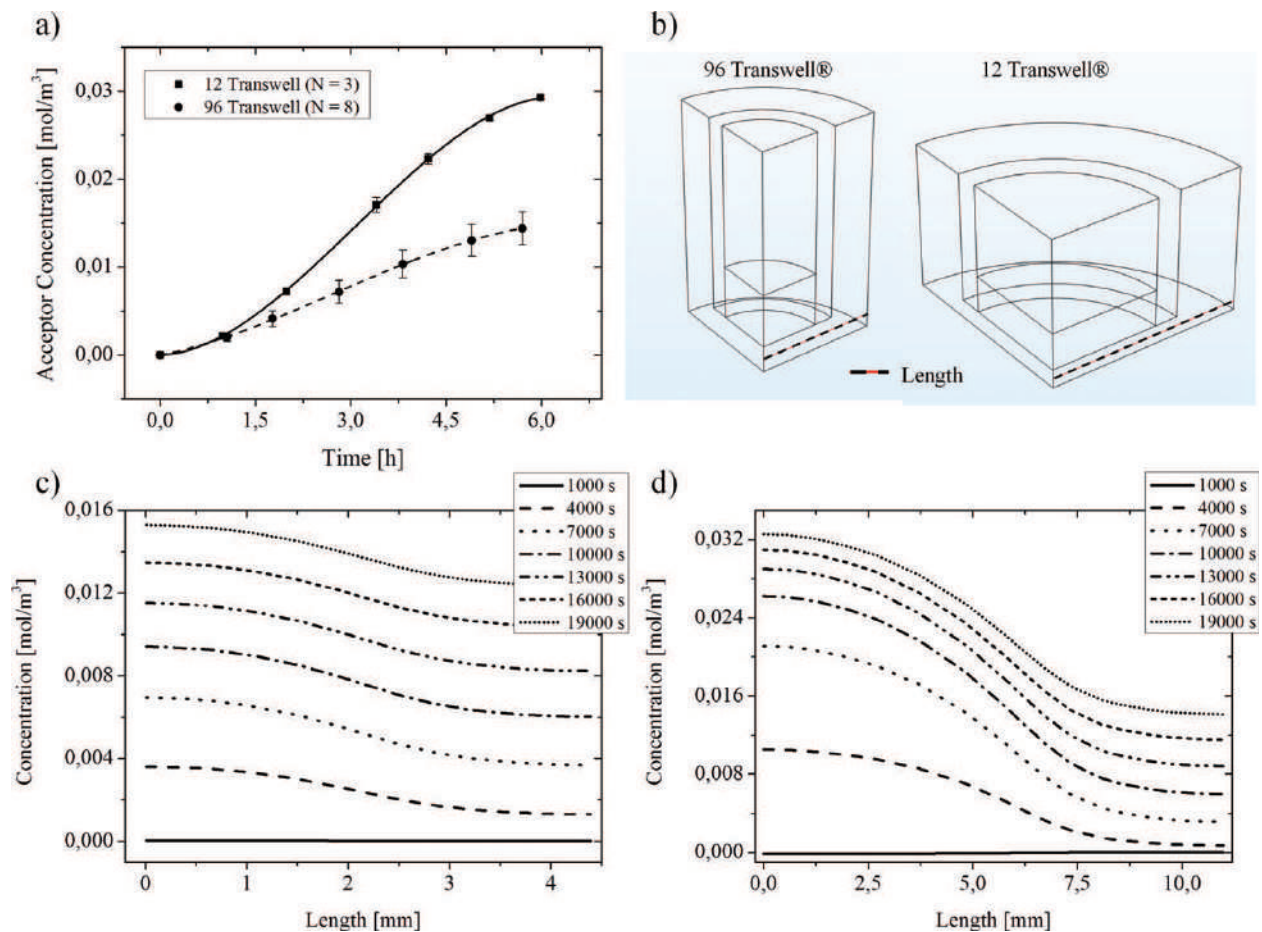
Figure 4. Permeation in 12- and 96-well membrane insert systems. (a) Experimental results of permeation of fluorescein sodium salt through 2% agarose. (b) Geometry of the 12 and 96 Transwell® system for the simulation and the position of the concentration measurement. (c) and (d) the concentration distribution at different time over the length at the red lined position on (b) ((c) 96 and (d) 12 Transwell® system).

a 12 Transwell® system. The 3D tissues consisted of a collagen matrix with different constellations of cell layers. Human primary fibroblasts were integrated into the collagen matrix and HaCaT cells were seeded on the top. A representative example of the 3D tissue is shown in **Figure 5**.

The results show that the permeation coefficient decreases when additional cell layers are added in the tissue model. The permeation coefficient of fluorescein sodium salt through collagen matrix (without cells) is 2.18×10^{-8} m/s, 1.85×10^{-8} m/s in tissue models with fibroblast and 1.67×10^{-8} m/s in models with HaCaT cells (see **Figure 6b)**. These results represent very well the barrier function of keratinocytes of the skin [3].

The particle size influences the permeation behavior through gels and biomaterials. It is well known that smaller molecules permeate faster through a matrix mesh than larger particles. This was already observed for permeation experiments through sclera [19], human epidermal membrane [45], human skin [33] and rat skin [3]. Fluorescein sodium salt and fluorescein iso-thiocyanate-dextrans (FITC-dextran) were used to vary the molecular size from 376 g/mol up
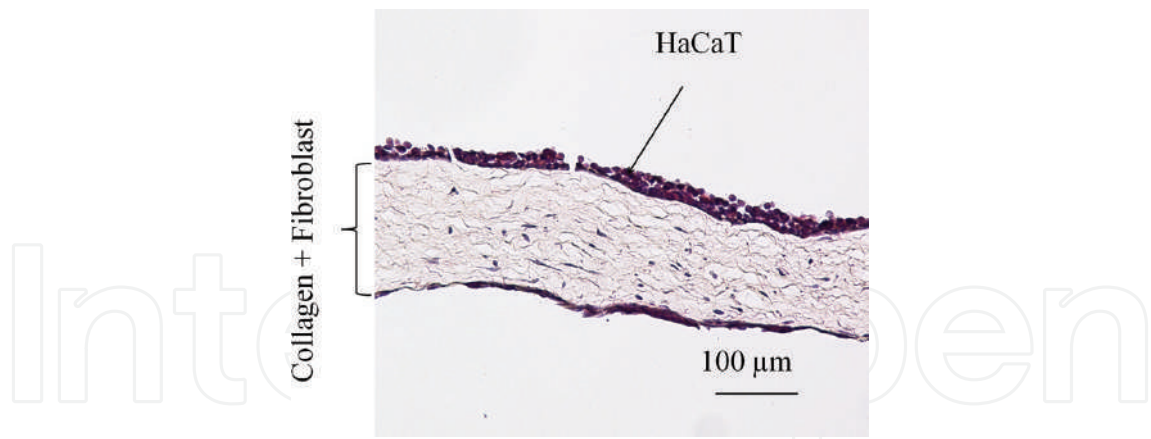
Figure 5. Hematoxylin and eosin stain of 3D tissue model consisting of collagen matrix with fibroblast and HaCaT seeded on the top.
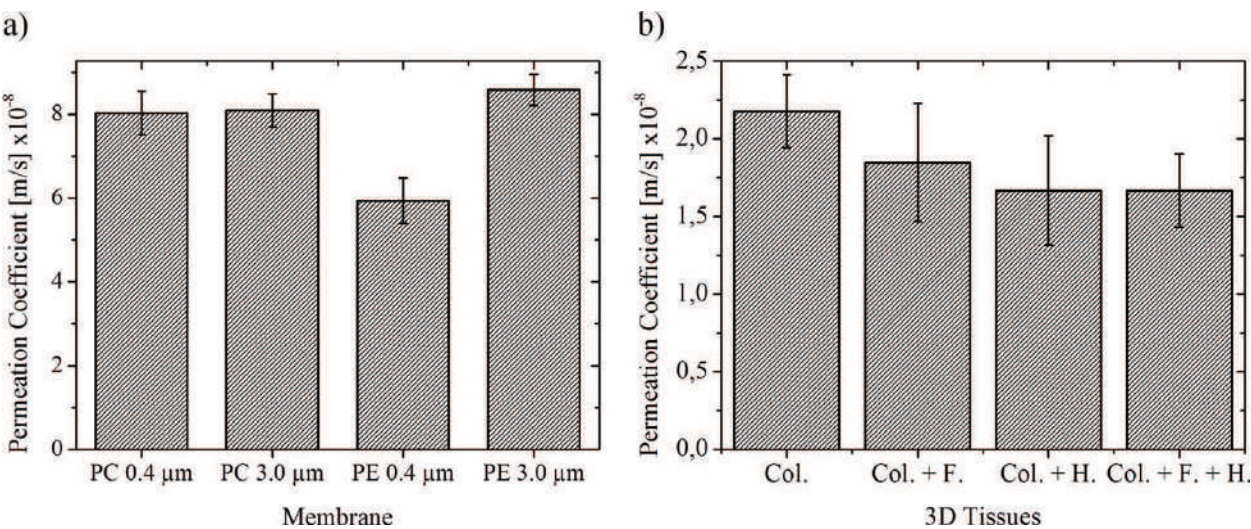

Figure 6. Permeation through different membranes and 3D skin tissues. (a) Results of permeation experiment with fluorescein sodium salt through 2% agarose gel on different membranes (n = 3). The 12 Transwell® system was used and membranes consisting of polycarbonate (PC) and polyethylene (PE) with pore sizes of 3.0 and 0.4 μm were tested. (b) Results of permeation experiments with fluorescein sodium salt through different 3D tissues in a 12 Transwell® system (n = 6). The 3D skin tissue consisted of collagen (Col.), collagen with primary human fibroblast (Col. + F.), collagen with HaCaTs (Col. + H.) and collagen with primary human fibroblast and HaCaTs (Col. F. + H.).

to 40,000 g/mol for permeation experiments in a 96 Transwell® system. The results show similar correlations between permeation coefficient and molecular size as the studies mentioned above. There is almost a linear relationship between these two factors, which is well described by the Navier–Stokes equation (see **Figure 7**). An exception is FITC-dextran 40,000 g/mol, which deviates from the linearity.

These experiments were simulated with COMSOL Multiphysics, where the diffusion coefficient is fitted on the experimental data. The simulation based on Fick's law is quite accurate for the permeation of substances with a small molecular size from 376 g/mol up to 4000 g/mol. The simulation shows good agreement with the experiment which is exemplary shown

in **Figure 8a**. In the case of larger molecular size, the simulation is different from experimental results. A closer look shows that the experimental data increased and flattened faster compared to the simulation (see **Figure 8b**). A possible reason for this effect could be the presence of particle size distribution in the substance. The migration of smaller particles reduces the lag time in the beginning of the permeation process, where large particles can increase the friction and slows down the diffusion. Especially the second effect leads to abnormal diffusion [46, 47]. This cannot be simulated with equations based on Fick's law.
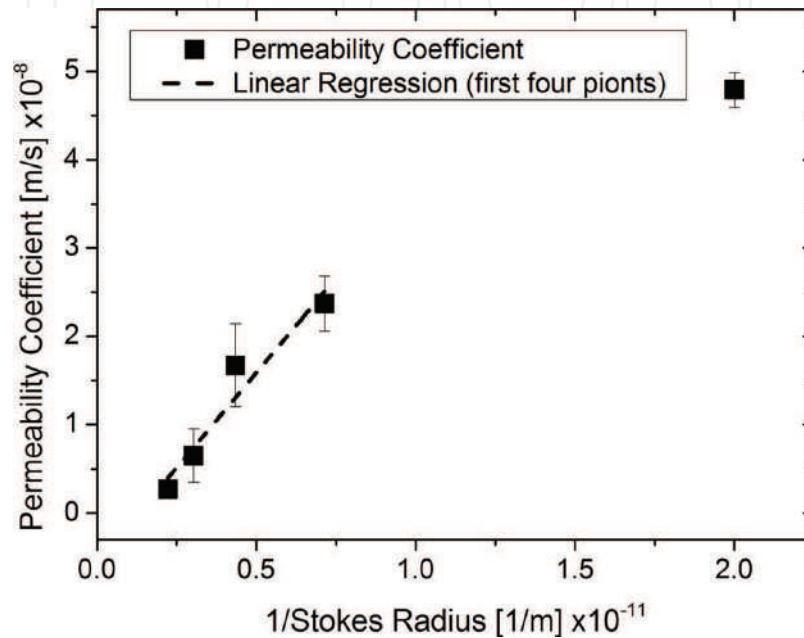
Figure 7. Permeability coefficient plotted over stokes radius. Results of permeation experiment in 96 Transwell® system with fluorescein sodium salt and FITC-dextran through 2% agarose gel.
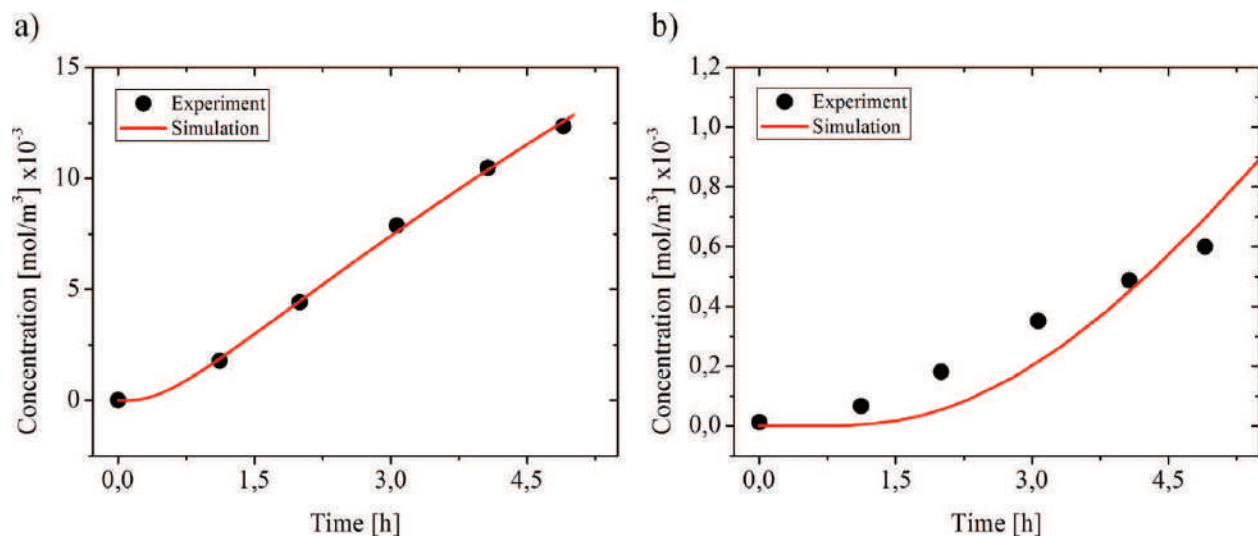

Figure 8. Simulation of permeation experiment with different molecular sizes. Results of permeation experiments and simulations with COMSOL **Multiphysics** of (a) fluorescein sodium salt and (b) FITC dextran 10,000 mg/mol in 96 Transwell systems through 2% agarose gel.

6. Conclusion and prospective

The studies have shown that the membrane insert system is a possible alternative for permeation studies. An advantage of the system is the small size. The membrane insert system of 96-well plates from CORNING has a cultivation surface of 0.143 cm^2 and a height of 2 cm. This reduces significantly the number of cells, materials and substances needed for the cultivation. In comparison to the Franz diffusion cell, the handling of such a system is easier and one experiment can be run with a large specimen number. A time-intensive mounting process of the samples (skin) is no longer required and the experiment can directly execute in the system. The sensitivity of this system is good enough to differ between 3D tissues as well as different cell layers and to detect different molecular sizes of the substance.

It should be considered that the permeation is detected through a membrane and the size of the system influences the permeation properties. The specimen has to cover up the whole membrane, otherwise the substance will pass by. Unlike the imaging and stripping method, it is not possible to measure the diffusion and penetration inside the membrane insert system. Alternatively, the diffusion can be calculated or estimated by simulation. Furthermore, this method can be used to investigate changes in the permeation behavior of the skin model during the cultivation or it can also be adapted for other systems, which use membrane insert systems. An example is the Two-Organ-on-a-Chip, a variant of TissUse's Multi-Organ-Chip platform [48–52]. This device enables the integration of skin models in a membrane insert system. Therefore this method can be used to investigate the permeation process into an organ-on-a-chip system in order to understand the substance distribution.

With the help of the simulation in COMSOL Multiphysics, it is possible to calculate the diffusion process in the membrane insert system. It is limited to small particle sizes and normal diffusion described by Fick's law. Otherwise, it is possible to optimize the simulation by integration of abnormal diffusion. Furthermore, the simulation is an attractive tool to support the experiments. On the one hand, it can be used to understand physical phenomena and to reduce experimental effort. On the other hand, it is modular and can be integrated into a more complex system to support permeation studies.

Acknowledgements

Appendices and nomenclatures

EC   European regulation

FITC dextran   fluorescein isothiocyanate-dextrans

FRAP	fluorescence recovery after photobleaching
FTIR	Fourier-transform-infrared
HaCaT	human adult low calcium high temperature
HSE	human skin equivalents
OECD	organization for economic co-operation and development

Author details

Hao-Hsiang Hsu[1], Katharina Schimek[2], Uwe Marx[2] and Ralf Pörtner[1]*

*Address all correspondence to: poertner@tuhh.de

1 Institute of Bioprocess and Biosystems Engineering, Hamburg University of Technology, Hamburg, Germany

2 TissUse GmbH, Berlin, Germany

References

[1] Ackermann K, Lombardi Borgia S, Korting H, Mewes K, Schäfer-Korting M. The Phenion® full-thickness skin model for percutaneous absorption testing. Skin Pharmacology and Physiology. 2010;**23**(2):105-112. DOI: 10.1159/000265681

[2] Asbill C. Evaluation of a human bio-engineered skin equivalent for drug permeation studies. Pharmaceutical Research. 2000;**17**(9):1092-1097. DOI: 10.1023/A:1026405712870

[3] Hadgraft J. Skin, the final frontier. International Journal of Pharmaceutics. 2001;**224**(1-2): 1-18. DOI: 10.1016/S0378-5173(01)00731-1

[4] Barry BW. Mode of action of penetration enhancers in human skin. Journal of Controlled Release. 1987;**6**(1):85-97. DOI: 10.1016/0168-3659(87)90066-6

[5] Valenzuela P, Simon JA. Nanoparticle delivery for transdermal HRT. Nanomedicine: Nanotechnology, Biology and Medicine. 2012;**8**:83-89. DOI: 10.1016/j.nano.2012.05.008

[6] Barbero AM, Frasch HF. Transcellular route of diffusion through stratum corneum: Results from finite element models. Journal of Pharmaceutical Sciences. 2006;**95**(10):2186-2194. DOI: 10.1002/jps.20695

[7] Bouwstra J, Pilgram G, Gooris G, Koerten H, Ponec M. New aspects of the skin barrier organization. Skin Pharmacology and Applied Skin Physiology. 2001;**14**:52-62. PubMed ID: 11509908

[8] Wertz PW. Lipids and barrier function of the skin. Acta Dermato-Venereologica. 2000; **208**:7-11. PubMed ID: 10884933

[9]   Tsukita S, Furuse M, Itoh M. Multifunctional strands in tight junctions. Nature Reviews. Molecular Cell Biology. 2001;**2**(4):285-293. DOI: 10.1038/35067088

[10]   Tsuruta D, Green KJ, Getsios S, Jonathan CRJ. The barrier function of skin: how to keep a tight lid on water loss. Trends in Cell Biology. 2002;**12**(8):355-357. PubMed ID: 12191905

[11]   Knorr F et al. Follicular transport route – Research progress and future perspectives. European Journal of Pharmaceutics and Biopharmaceutics. 2009;**71**(2):173-180. DOI: 10.1016/j.ejpb.2008.11.001

[12]   Schaefer H, Lademann J. The role of follicular penetration. Skin Pharmacology and Applied Skin Physiology. 2001;**14**:23-27. DOI: 10.1159/000056386

[13]   Lademann J et al. Hair follicles—An efficient storage and penetration pathway for topically applied substances. Skin Pharmacology and Physiology. 2008;**21**(3):150-155. DOI: 10.1159/000131079

[14]   Otberg N et al. The role of hair follicles in the percutaneous absorption of caffeine. British Journal of Clinical Pharmacology. 2008;**65**(4):488-492. DOI: 10.1111/j.1365-2125.2007.03065.x

[15]   Wilkinson DS. Mass transport in solids and fluids. Cambridge University Press. 2000. ISBN: 9780521624947

[16]   Cussler EL. Diffusion: Mass Transfer in Fluid Systems. 2nd ed. Cambridge University Press; 1997. ISBN: 0-521-45078-0

[17]   Crank J. The Mathematics of diffusion. 2nd ed. Oxford, Clarendon Press; 1975. ISBN: 0-19-853411-6

[18]   Netzlaff F et al. Permeability of the reconstructed human epidermis model Episkin® in comparison to various human skin preparations. European Journal of Pharmaceutics and Biopharmaceutics. 2007;**66**(1):127-134. DOI: 10.1016/j.ejpb.2006.08.012

[19]   Jayakrishna A et al. Diffusion of high molecular weight compounds trough Sclera. IOVS. 2000;**41**(5):1181-1185. DOI: b, 19.02.2015

[20]   Ackermann K, Lombardi Borgia S, Korting H, Mewes K, Schäfer-Korting M. The Phenion® full-thickness skin model for percutaneous absorption testing. Skin Pharmacology and Physiology. 2010;**23**(2):105-112. DOI: 10.1159/000265681

[21]   Bran B et al. A new discriminative criterion for the development of Franz diffusion tests for transdermal pharmaceuticals. Journal of Pharmaceutical Sciences. 2010;**13**(2):218-230. DOI: 10.18433/J3WS33

[22]   Pineau A, Guillard O, Favreau F, Marrauld A, Fauconneau B. In vitro study of percutaneous absorption of aluminum from antiperspirants through human skin in the Franz diffusion cell. Journal of Inorganic Biochemistry. 2012;**110**:21-26. DOI: 10.1016/j.jinorgbio.2012.02.013

[23] Larese Filon F et al. In vitro percutaneous absorption of cobalt. International Archives of Occupational and Environmental Health. 2004;(2):85-89. DOI: 10.1007/s00420-003-0455-4

[24] Ng S-F, Rouse JJ, Sanderson FD, Meidan V, Eccleston GM. Validation of a static Franz diffusion cell system for in vitro permeation studies. AAPS PharmSciTech. 2010;**11**(3):1432-1441. DOI: 10.1208/s12249-010-9522-9

[25] Bonferoni MC, Rossi S, Ferrari F, Caramella C. A modified Franz diffusion cell for simultaneous assessment of drug release and Washability of Mucoadhesive gels. Pharmaceutical Development and Technology. 1999;**4**(1):45-53. DOI: 10.1080/10837459908984223

[26] Bartosova L, Bajgar J. Transdermal drug delivery in vitro using diffusion cells. CMC. 2012;**19**(27):4671-4677. DOI: 10.2174/092986712803306358

[27] Pluen A, Netti PA, Jain RK, David A, Berk DA. Diffusion of macromolecules in agarose gels: Comparison of linear and globular configurations. Biophysical Journal. 1999;**77**(1):542-552. DOI: 10.1016/S0006-3495(99)76911-0

[28] Cornelissen LH, Bronneberg D, Oomens CWJ, Baaijens FPT. Diffusion measurements in epidermal tissues with fluorescent recovery after photobleaching. ISBS. 2008;**14**(4):462-467. DOI: 10.1111/j.1600-0846.2008.00313.x

[29] Leddy HA, Guilak F. Site-specific molecular diffusion in articular cartilage measured using fluorescence recovery after Photobleaching. Annals of Biomedical Engineering. 2003;**31**(7):753-760. DOI: 10.1114/1.1581879

[30] Seiffert S, Oppermann W. Systematic evaluation of FRAP experiments performed in a confocal laser scanning microscope. Journal of Microscopy. 2005;**220**(1):20-30. DOI: 10.1111/j.1365-2818.2005.01512.x

[31] Pirot F, Kalia YN, Stinchcomb AL, Keating G, Bunge A, Guy RH. Characterization of the permeability barrier of human skin in vivo. Proceedings of National Academy of Sciences USA. 1997;**94**:1562-1567. 0027-8424/97/941562-6$2.00/0

[32] Tetteh J et al. Local examination of skin diffusion using FTIR spectroscopic imaging and multivariate target factor analysis. Analytica Chimica Acta. 2009;**642**(1-2):246-256. DOI: 10.1016/j.aca.2009.03.002

[33] Guldbrand S et al. Two-photon fluorescence correlation spectroscopy as a tool for measuring molecular diffusion within human skin. European Journal of Pharmaceutics and Biopharmaceutics. 2013;**84**(2):430-436. DOI: 10.1016/j.ejpb.2012.10.001

[34] Berland KM, So PT, Gratton E. Two-photon fluorescence correlation spectroscopy: Method and application to the intracellular environment. Biophysical Journal. 1995;**68**(2):694-701. DOI: 10.1016/S0006-3495(95)80230-4

[35] Ghosn MG et al. Monitoring of glucose permeability in monkey skin in vivo using optical coherence tomography. Journal of Biophotonics. 2010;**3**(1-2):25-33. DOI: 10.1002/jbio.200910075

[36] Teichmann A et al. Differential stripping: Determination of the amount of topically applied substances penetrated into the hair follicles. The Journal of Investigative Dermatology. 2005;**125**(2):264-269. DOI: 10.1111/j.0022-202X.2005.23779.x

[37] Surber C, Schwarb FP, Smith EW. Tape-stripping technique. Cutaneous and Ocular Toxicology. 2002;**20**(4):461-474. DOI: 10.1081/CUS-120001870

[38] Weigmann H-J, Lademann MH, Schaefer H, Sterry W. Determination of the horny layer profile by tape stripping in combination with optical spectroscopy in the visible range as a prerequisite to quantify percutaneous absorption. Skin Pharmacology and Physiology. 1999;**12**(1-2):34-45. DOI: 10.1159/000029844

[39] Jacobi U, Weigmann H-J, Ulrich J, Sterry W, Lademann J. Estimation of the relative stratum corneum amount removed by tape stripping. ISBS. 2005;**11**(2):91-96. DOI: 10.1111/j.1600-0846.2005.00094.x

[40] Macfarlane M et al. A tiered approach to the use of alternatives to animal testing for the safety assessment of cosmetics: Skin irritation. Regulatory Toxicology and Pharmacology. 2009;**54**(2):188-196. DOI: 10.1016/j.yrtph.2009.04.003

[41] Basketter D, Jírova D, Kandárová H. Review of skin irritation/corrosion hazards on the basis of human data: A regulatory perspective. Interdisciplinary Toxicology. 2012;**5**(2):98-104. DOI: 10.2478/v10102-012-0017-2

[42] York M, Griffiths HA, Whittle E, Basketter DA. Evaluation of a human patch test for the identification and classification of skin irritation potential. Contact Dermatitis. 1996;**34**(3):204-212

[43] Prunieras M, Regnier M, Woodley D. Methods for cultivation of keratinocytes with an air-liquid Interface. The Journal of Investigative Dermatology. 1983;**81**:28-33. DOI: 10.1111/1523-1747.ep12540324

[44] Mathes SH, Ruffner H, Graf-Hausner U. The use of skin models in drug development. Advanced Drug Delivery Reviews. 2014;**69-70**:81-102. DOI: 10.1016/j.addr.2013.12.006

[45] Peck KD, Ghanem A, Higuchi WI. Hindered diffusion of polar molecules through and effective pore radii estimates of intact and ethanol treated human epidermal membrane. Pharmaceutical Research. 1994;**11**(9):1306-1314. DOI: 10.1023/A:1018998529283

[46] Laurent TC, Sundelöf L-O, Wik KO, Wärmegard B. Diffusion of dextran in concentrated solutions. European Journal of Biochemistry. 1976;**68**:95-102. DOI: 10.1111/j.1432-1033.1976.tb10767.x

[47] Metzler R, Klafter J. The random walk's guide to anomalous diffusion: A fractional dynamics approach. Physics Reports. 2000;**339**(1):1-77. DOI: 10.1016/S0370-1573(00)00070-3

[48] Ataç B et al. Skin and hair on-a-chip: In vitro skin models versus ex vivo tissue maintenance with dynamic perfusion. Lab on a Chip. 2013;**13**(18):3555-3561. DOI: 10.1039/c3lc50227a

[49] Maschmeyer I et al. Chip-based human liver–intestine and liver–skin co-cultures – A first step toward systemic repeated dose substance testing in vitro. European Journal of Pharmaceutics and Biopharmaceutics. 2015;**95**:77-87. DOI: 10.1016/j.ejpb.2015.03.002

[50] Materne E-M et al. The multi-organ Chip - a microfluidic platform for long-term multi-tissue coculture. JoVE. 2015;**98**:1-11. DOI: 10.3791/525264

[51] Schimek K et al. Integrating biological vasculature into a multi-organ-chip microsystem. Lab on a Chip. 2013;**13**(18):3588. DOI: 10.1039/c3lc50217a

[52] Wagner I et al. A dynamic multi-organ-chip for long-term cultivation and substance testing proven by 3D human liver and skin tissue co-culture. Lab on a Chip. 2013;**13**(18):3538. DOI: 10.1039/c3lc50234a

[53] Hsu H et al. A method for determination and simulation of permeability and diffusion in a 3D tissue model in a membrane insert system for multi-well plates. JOVE. 2017 https://www.jove.com/video/56412/a-method-for-determination-simulation-permeability-diffusion-3d

We are IntechOpen,
the world's leading publisher of
Open Access books
Built by scientists, for scientists

6,300
Open access books available

171,000
International authors and editors

190M
Downloads

Our authors are among the

154
Countries delivered to

TOP 1%
most cited scientists

12.2%
Contributors from top 500 universities

CLARIVATE ANALYTICS
BOOK CITATION INDEX
INDEXED

WEB OF SCIENCE™

Selection of our books indexed in the Book Citation Index
in Web of Science™ Core Collection (BKCI)

Interested in publishing with us?
Contact book.department@intechopen.com

Numbers displayed above are based on latest data collected.
For more information visit www.intechopen.com

Biomaterials for Tendon/Ligament and Skin Regeneration

Xingguo Cheng

Additional information is available at the end of the chapter

Abstract

Tendon/ligament injury or skin injuries due to diseases, trauma, and surgery are common. Timely functional repair and tissue regeneration is a key to improve the quality of life of the patient while reducing health care cost. Tendon/ligament/skin is also enriched in a common extracellular matrix (ECM), collagen I, III, and elastin. Tissue engineering and regenerative medicine, the combination of (stem) cells, growth factors, and biomaterial scaffolds, is an emergent field, which has attracted substantial attention over the years. Biomaterials are considered the foundation of regenerative medicine. A key to find a new solution to tendon/ligament/skin healing is to synthesize new functional biomaterials, which have better biomechanical properties, biodegradability, and cell supporting properties. This chapter will review existing FDA-approved biomaterial-based therapy, as well as those in development.

Keywords: biomaterials, tendon, skin, regeneration

1. Introduction

From material science point of view, tendon/ligament and skin tissue are similar in that they are mainly composed of collagen and elastin. Up to 80% of the dry weight is collagen type I. However, their micro and hierarchical structures and functions are very different from each other. Tendon/ligament is composed of densely packed, aligned collagen fiber bundles, whereas skin is composed of a layered structure of collagen random naonfibril network. **Table 1** summarizes the key properties of tendon/ligament and skin tissue in human.

The regeneration of a large size, lost tendon/ligament, and skin tissue normally involves a type of stem cells/progenitor cells of endogenous origin or exogenous origin combined with a

	Tendon/ligament	Skin
Main composition	>80% Collagen, ~5% elastin elastin	>80% Collagen, ~5% elastin
Minor composition	Fibronectin, proteoglycan	Fibronectin, proteoglycan
Main cells	Fibroblast	Fibroblast and keratinocytes
Vasculature	Few	Abundant
Structure	1D Aligned fiber bundles (nano-macro)	2D random nanofibrils (weave basket pattern)
Mechanical properties	Strong and elastic	Weak and elastic

Table 1. A general comparison of two different connective tissues: tendon/ligament and skin.

biomaterial. Stem cells can be derived from tendon/ligament or skin, or from embryo, placenta, adipose tissue, bone marrow, umbilical cord, etc. This review focuses only on regeneration using exogenous stem cells coupled with a biomaterial matrix/carrier implanted to the wound site. Biomaterial can play a key role in protection of the cells from dehydration while it serves as a temporary substrate for stem cells to proliferate, or differentiate, and synthesize tissue-specific matrix. The morphology, topography, composition, stiffness of biomaterials may play a key role in controlling the differentiation of stem cells, in addition to biochemical factors, mechanical cues, or genetic/cellular cues. This chapter focuses on biomaterial explored for tendon/ligament/skin tissue regeneration applications.

1.1. Research methods

We performed a comprehensive search of PubMed using keywords "tendon," "ligament," "skin," "regeneration," "scaffold", over the years 1970–2016. All articles relevant to the subject were retrieved, and their bibliographies hand searched for further references in the context to biomaterials for tendon/ligament/skin regeneration

2. Results

2.1. Biomaterial directly derived from patients

2.1.1. PRP

Platelet-rich plasma (PRP) is derived from blood and PRP gel is widely used for tendon/ligament repair. Recently, PRP was combined with adipose-derived stem cells (ADSCs) and it was found that PRP combined with stem cells resulted in improved mechanical strength in a rabbit tendon model compared to PRP gel alone [1]. Similar results were also observed using PRP with tendon-derived stem cells (TDSCs) [2]. However, in a sheep model, no differences were observed between the PRP group and PRP-stem cell group [3]. This approach is highly translational, since both autologous stem cells and PRP can be obtained from the same patients. The concern may be the leucocytes-containing PRP (L-PRP) that have a catabolic

effect, whereas pure PRP (P-PRP) without leucocytes have anabolic effects and results in over-proliferation and scar tissue formation. The complex interaction between PRP and stem cells may explain the different preclinical outcome and warrant a large random clinical trial.

2.1.2. Fibrin

Fibrin can be derived from human plasma. After addition of thrombin, it will form a gel, a process used for blood clotting. Stem cells can be added together with fibrin and thrombin and sprayed onto the wound for the promotion of wound closure and healing. The fibrin combined with bone marrow stem cells spray was successfully tested to prevent ulceration and accelerate wound closure in mice [4]. A small human clinical trial showed this approach accelerates wound closure and resurfacing without adverse effects [5]. Poly(ethylene glycol) PEG-modified fibrin combined with adipose-derived stem cells (ADSCs) also showed promising results in a pig burn model [6].

2.1.3. Amniotic membrane

Human placenta-derived biomaterial is unique in that it has immune privilege while it contains multiple growth factors. Human ADSCs (hADSCs) seeded onto radiosterilized human amnion are viable and can proliferate. These cells are able to migrate over these scaffolds as demonstrated by using time-lapse microscopy. In addition, the scaffolds induce hADSCs to secrete interleukin-10, an important negative regulator of inflammation [7]. This suggests that placenta-derived biomaterial may be a good substrate for stem cells and used for skin/tendon applications.

3D micronized (300–600 µm) amniotic membrane (mAM) was made by means of repeated freeze-thawing cycles to deplete cell components and homogenized with a macrohomogenizer in liquid nitrogen. These mAM loaded with epidermal stem cells (ESCs) (ESC-mAM) was further transplanted to full-thickness skin defects in nude mice. ESCs survived well and formed a new epidermis. Four weeks after transplantation, papilla-like structures were observed, and collagen fibers were well and regularly arranged in the newly formed dermal layer. In conclusion, the mAM as a novel natural microcarrier possesses an intact basement membrane structure and bioactivities [8].

2.2. FDA-approved ECM grafts for tendon augmentation and skin regeneration

A recent study showed that decellularized matrix from different tissues (tendon, bone, and skin) affect the differentiation of stem cell in a different way. Decellularized bone matrix may induce the undesirable osteogenic differentiation of stem cells, while tendon or skin matrix does not have such an effect [9]. The ECM components provide a niche for proper differentiation of stem cells. For example, ECM without biglycan (Bgn) and fibromodulin (Fmod) will affect the differentiation of tendon stem cells by modulating bone morphogenetic protein signaling and impairs tendon formation *in vivo* [10]. Autologous origin, but decelluarized dermal matrix using trypsin and Trion X-100, after combined with ADSCs, was found to enhance wound healing in a murine model of a full-thickness skin defect [11].

Many FDA-approved human or animal decelluarized tissue matrixes have been approved for direct tendon/ligament/skin repair without any (stem) cells (**Table 2**). The key advantages of decellularized tissue grafts are that they largely maintain the main architecture, composition, and mechanical properties of native tissues. These allografts/xenografts are processed to remove immunogenic cells, DNAs, and certain immunogenic molecules. Typical problems are that these grafts are slower to repair the tissue and some fail to restore the proper functions (e.g., scarring). For tissue regeneration using these ECM biological grafts, stem cells may need to be reseeded onto the grafts for recellularization. For a dense tendon allograft, direct cell seeding may be difficult. The recellularization onto the surface may be achieved using a cell-loaded gel coating [12]. However, it is highly desirable to get cells inside the grafts as well. Thus, ECM grafts may be processed to have a much higher porosity than the original tissue. Proration/incision into the ECM grafts may help the penetration of cells and nutrients. Instead of being coated with cell-laden gel, an interesting approach is to use a stem cell-sheet to wrap around a frozen tendon graft for implantation [13]. Interesting, a case report showed that a dermal allograft combined with PRP and autologous mesenchymal stem cells (MSCs) derived from peripheral blood (PB-MSCs) resulted in enhanced healing of human rotator cuff [14].

Some of the FDA-approved ECM biomatrices were combined with stem cells, and investigated for tendon/ligament/skin regeneration applications. Human acellular allograft (Alloderm) was investigated for direct cell seeding using ADSCs. It was concluded that human ADSCs can attach to Alloderm with the dermis side up in a petri dish [15]. ADSC seeded onto Alloderm was also implanted *in vivo* for skin regenerations with promising results [16]. Strattice was evaluated for seeding with rat MSCs [17]. Thus, the stem cell-seeded biologic graft can be used as a tendon wrap or a skin regeneration material. A study was performed to compare the survival and proliferation of stem cells via bioluminescent imaging. The use of biologic graft

Alloderm	Human skin (decelluarized)
GraftJacket	Human skin
Restore	10-layered porcine small intestine submucosa (SIS) treated with peracetic acid/ethanol (90% collagen, 5–10% lipids)
TissueMend	Noncrosslinked fetal biovine dermal matrix [19]
BioBlanket	Crosslinked porous bovine dermis
Permacol or Zimmer collagen repair patch	Porcine acelluar dermis treated with trypsin, solvent, and crosslinked with hexamethylene diisocyanate (HMDI)
Strattice	Porcine acelluar dermal matrix
Cuffpatch	EDC-crosslinked matrix from eight layers of treated SIS (97% collagen, 2% elastin)
OrthoADAPT	Crosslinked equine pericardium (90% collagen I, 10% collagen II)

Table 2. An example list of biologic ECM grafts with potential for tendon/skin regeneration.

patch (SIS) as carrier of ADSCs significantly increases the survival of stem cells as compared to direct injection of ADSCs into the skin wounds [18]. There may be a synergistic angiogenesis promoting effects of biologic graft with stem cells, which may be important for tendon/skin wound healing [19].

Another interesting approach is to use ECM directly secreted by the cells as a carrier for stem cells. For example, stem cells can be incubated at 37°C in a temperature-responsive flask (e.g., upcell™, Cellseed, Japan) and they will product ECM after addition of ascorbic acid. The cell sheets can be lifted at room temperature since the Poly-n-isopropylacrylamide (Poly-NIPAM)-based substrate will become soluble at lower temperature. The cell-ECM sheet has been explored for promotion of tendon/ligament healing [20] as well as diabetic skin wound healing [21].

2.3. FDA-approved biomaterial

2.3.1. Collagen sponge scaffold

(5 mm × 2 mm) collagen sponge scaffolds (Zimmer Dental) were used for the culture of (BM) MSCs. Cell-seeded scaffolds were placed in culture dishes and incubated for 2 hours in a minimum volume of growth medium, after which more medium was applied to submerge the scaffolds. After an additional 24-hour culture, cells seeded in scaffolds were treated with 10 ng/mL of recombinant (BMP) 12 for 12 hours. The medium was then replaced with fresh growth medium and scaffolds were either cultured for an additional 7 days or immediately implanted into partial calcaneal tendon defects in rats. It was shown that after 21 days, the BMP12-treated, collagen-cell scaffold results in robust formation of tendon-like tissue [22]. Similarly, a collagen carrier combined with ASDCs showed they did not improve the biomechanical properties of the tendon-to-bone healing. However, the ADSCs group showed less inflammation, which may lead to a more elastic repair and less scarred healing in a rat model.

2.3.2. Integra bilayer

Integra® bilayer wound Matrix (LifeSciences Corp., Plainsboro, New Jersey) is a dermal acellular analog composed of bovine collagen type I crosslinked with glycosaminoglycans. Importantly, inclusion of WJ-MSC into Integra induced significant up-regulation of prototypical angiogenic and healing factors, stimulating pleiotropic aspects of neovascularization in experimental settings of angiogenesis, without altering the inflammatory response in the animals, thus demonstrating their potential benefit in therapeutic care of wounds and skin grafts [23]. Recently, Integra dermal matrix scaffold engineered with adult mesenchymal stem cells and platelet-rich plasma was investigated *in vitro* and demonstrated promising preliminary results [24].

2.4. Synthetic biopolymer matrix

Biopolymer matrix such as collagen, gelatin, hyaluronic acid, chitosan, silk, cellulose are the essential ECM components of human, animal, or plant cells. They have showed great promise for attachment, proliferation, and differentiation of stem cells and have been explored for tendon and skin regeneration.

2.4.1. Collagen

Collagen monomer solution can be extracted from skin of fetal bovine calf in close herd. Collagen-based biomaterial has been widely used for tendon/skin regeneration. For tendon application, it is highly desirable to prepare aligned collagen fiber scaffolds. Anisotropic collagen biomaterial can be prepared by directional freeze drying [25], electrospinning, or a novel process called electrochemical process. Electrochemically aligned collagen fiber and skin substrate have been coupled with stem cells for both tendon [26] and skin regeneration [27], respectively. Collagen carrier/gel [28] or collagen combined with stem cell accelerated the wound healing in healing-impaired db/db mice [29].

2.4.2. Pullulan-collagen hydrogel

A biomimetic pullulan-collagen hydrogel was used to create a functional biomaterial-based stem cell niche for the delivery of MSCs into wounds. Murine bone marrow-derived MSCs were seeded into hydrogels and compared to MSCs grown in standard culture conditions. Hydrogels induced MSC secretion of angiogenic cytokines and expression of transcription factors associated with maintenance of pluripotency and self-renewal. MSC-seeded hydrogels showed significantly accelerated healing and a return of skin appendages [30].

2.4.3. Gelatin

Gelatin is denatured collagen. Human ADSCs laden gelatin microcryogels (GMs) were evaluated *in vitro* as a stem cell carrier. The cell phenotype markers, stemness genes, differentiation, secretion of growth factors, cell apoptosis, and cell memory were compared against cells without a carrier. The priming effects of GMs on upregulation of stemness genes and improved secretion of growth factors of hASCs were demonstrated.

2.4.4. Hyaluronic acid (HA)

Hyaluronic acid (HA) is a nonsulfated, linear polysaccharide with the repeating disaccharide, β-1,4-D-glucuronic acid - β-1,3-N-acetyl-D-glucosamine (Mw: 100–8000 KDa). It is an ECM component. ADSCs combined with hyaluronic acid (ADSC-HA) dermal filler were implanted in rats and compared with HA alone. It was demonstrated that ADSC-HA has better filling effects than HA alone. A total of 70% of stem cells remain in the injection site after 3 months. These suggested stem cells have the potential to improve the esthetic effects and longevity of dermal fillers [31].

2.4.5. Chitin/Chitosan

Chitosan-hyaluron membrane: Hsu et al. investigated adult ADSCs spheroids combined with a chitosan-hyaluron membrane and showed biomaterial combined with stem cells promoted wound healing in a rat skin repair model [32]. Dense and porous chitosan-xanthan membranes seeded with multipotent mesenchymal stromal cells were evaluated for the treatment of skin wounds. The membranes showed to be nonmutagenic and allowed efficient adhesion

and proliferation of the mesenchymal stromal cells *in vitro*. *In vivo* assays performed with mesenchymal stromal cells grown on the surface of the dense membranes showed acceleration of wound healing in Wistar rats [33].

2.4.6. Gelatin/PEG

A thiol-ene Michael-type addition was utilized for rapid encapsulation of MSCs within a gelatin/PEG biomatrix according to Eq. (1). The MSCs/gelatin/PEG biomatrix was applied as a provisional dressing to full-thickness wounds in Sprague-Dawley rats. Biomatrix resulted in attenuated immune cell infiltration, lack of foreign giant cell (FBGC) formation, accelerated wound closure and re-epithelialization, as well as enhanced neovascularization and granulation tissue formation by 7 days [34].

$$\text{Gelatin - PEG - SH} + \text{PEG-diacrylate} \; \rightarrow \; \text{Gelatin - PEG hydrogel} \tag{1}$$
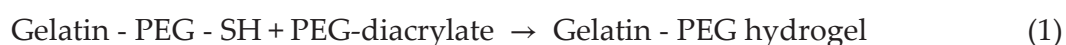
2.4.7. Silk

Electrospun nanofiberous scaffolds prepared from silk fibroin protein were seeded with bone marrow-derived mesenchymal stem cells (MSCs) and epidermal stem cells (ESCs). The constructs were evaluated for wound re-epithelization, collagen synthesis, as well as the skin appendages regeneration. It was shown that both the transplantation of MSCs and ESCs could significantly accelerate the skin re-epithelization, stimulate the collagen synthesis. Furthermore, the regenerative features of MSCs and ESCs in activating the blood vessels and hair follicles formation, respectively, were suggested [35]. Combination of silk with collagen or poly(lactic-co-glycolic acid) (PLGA) [18] and stem cells were evaluated in a rabbit tendon defect model [36].

2.4.8. Fibrin-agarose

A stroma skin substitute was first generated by using a mixture of human fibrin obtained from frozen human plasma and 0.1% agarose. An average of 250,000 cultured skin fibroblasts were added to 5 mL of the mixture immediately before inducing the polymerization of the artificial stroma on Transwell (Corning Enterprises, Corning, NY, http://www.corning.com) porous inserts. Once the stromas jellified, human umbilical cord Wharton's jelly stem cells (HWJSCs) were seeded on top of the skin artificial stromas and cultured. It was demonstrated that this 3D bioactive scaffold can stratify and form epithelial cell-like layers and well-formed cell-cell junctions [37]. The authors also demonstrated similar strategy can be used for regeneration of oral mucosa using human Wharton's jelly stem cells (HWJSCs)-seeded fibrin-agarose-mucosal fibroblasts.

2.4.9. Sodium carboxymethylcellulose (CMC)

Sodium CMC was evaluated as a substrate for ADSCs and implanted in adult male Wistar rats. CMC at 10 mg/mL associated with ADSCs increased the rate of cell proliferation of the granulation tissue and epithelium thickness when compared to untreated lesions (Sham).

CMC is capable to allow the growth of ADSCs and is safe for this biological application up to the concentration of 20 mg/mL. These findings suggest that CMC is a promising biomaterial to be used in cell therapy [38].

2.5. Synthetic nondegradable polymer-based biomaterial

Table 3 summarizes common nondegradable polymer used as a biomaterial or as a modifier of ECM-based biopolymer for skin and tendon tissue engineering applications. The incorporation of such polymer allows biopolymer (collagen, gelatin, HA) to be able to gelled at physiological condition (e.g., under UV/blue light, ambient temperature, or room temperature aqueous free radical initiator. Stem cells can be directly encapsulated inside the substrate during gel formation.

2.5.1. Poly(NIPAM)-based

A biodegradable, multifunctional crosslinker and an n-isopropylacrylamide (NIPAM)-based, thermosensitive hydrogel was synthesized to carry BMSCs to treat diabetic skin ulcers. The crosslinker contains an arginylglycylaspartic acid(GRD)-like motif that promotes cell attachment and differentiation of BMSCs. After hydrogel association with BMSCs treated the diabetic skin wound in mice, significantly greater wound contraction was observed in the hydrogel + BMSCs group. Histology and immunohistochemistry results confirmed that this treatment contributed to the rapid healing of diabetic skin wounds by promoting granulation tissue formation, angiogenesis, extracellular matrix (ECM) secretion, wound contraction, and re-epithelialization. These results show that a hydrogel laden with BMSCs may be a promising therapeutic strategy for the management of diabetic ulcers [39].
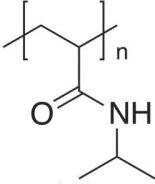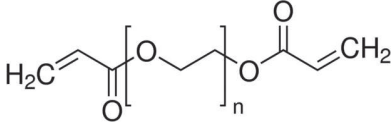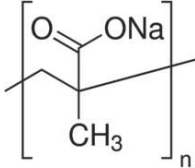
Poly(NIPAM)	PEGDA	Poly(methyl acrylate) (PMA)

Table 3. Common synthetic, nondegradable polymer used as hydrogel or gel components.

2.6. Polyester-based degradable polymer biomaterial

The structure of common polyester is shown in **Table 4**. Stem cell-coated polyester suture was evaluated for tendon applications in a rat model [40]. Electrospun PLGA fiber may be more suitable for tendon regeneration than film [41]. (PGA/PLA) fiber combined with ADSCs improve tendon in a rabbit tendon model [42]. Open cell PLGA seeded with stem cells produced more collagen type I [43]. Knited PLGA encapsulated with stem cell/alginate gel [44]. PGA sheet with MSCs were able to regenerate tendon-bone insertions and the tendon in rabbit [45]. Electrospun polycaprolactone/gelatin (PCL/GT) membrane and human urine-derived stem cells (USCs) were evaluated for skin wound healing in a rabbit model [46]. USCs-PCL/GT-treated wounds closed much faster, with increased re-epithelialization, collagen formation, and
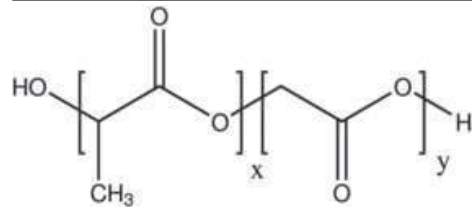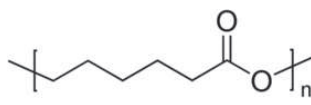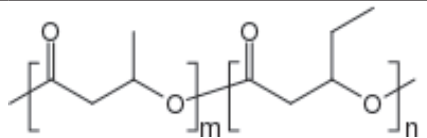
PLGA	PCL	PHBV

Table 4. Common synthetic, degradable polymer used for tendon/skin regeneration applications.

angiogenesis. Moreover, USCs could secrete vascular endothelial growth factor(VEGF) and transforming growth factor (TGF)-β1, and USC-conditioned medium enhanced the migration, proliferation, and tube formation of endothelial cells. This data suggested that USCs in combination with PCL/GT significantly prompted the healing of full-thickness skin wounds in rabbits. Similarly, electrospun poly (L-lactide-co-ε-caprolactone)/poloxamer (PLCL/P123) scaffolds combined with ADSCs enhanced skin wound healing in a rat model [47]. Chitosan-crosslinked poly (3-hydroxybutyrate-co-3-hydroxyvalerate) (PHBV) was used to load unrestricted somatic stem cells. The cell-laden scaffold showed better results during the healing process of skin defects in rat models [48, 49].

3. Conclusion

Biomaterials play an important role for attachment, survival, and function of stem cells. Many biomaterials are either used alone or as one component of the product for the regeneration of tendon/ligament/skin. Despite abundance of biomaterial developed, the optimal biomaterials that meet the structural, mechanical, functional requirement of tendon/ligament tissues to be regenerated remain a challenge. Novel biomaterial fabrication process, biomaterial design, and biomaterial synthesis toward tendon/ligament and skin regeneration are urgently needed.

Author details

Xingguo Cheng

Address all correspondence to: xcheng@swri.org

Southwest Research Institute, San Antonio, TX, USA

References

[1] Uysal CA, et al. Adipose-derived stem cells enhance primary tendon repair: Biomechanical and immunohistochemical evaluation. Journal of Plastic Reconstructive & Aesthetic Surgery. 2012:**65**(12):1712-1719

[2] Xu K, et al. Platelet-rich plasma activates tendon-derived stem cells to promote regeneration of Achilles tendon rupture in rats. Journal of Tissue Engineering and Regenerative Medicine. 2017;**11**(4):1173-1184

[3] Martinello T, et al. Effects of *in vivo* applications of peripheral blood-derived mesenchymal stromal cells (PB-MSCs) and platlet-rich plasma (PRP) on experimentally injured deep digital flexor tendons of sheep. Journal of Orthopaedic Research. 2013;**31**(2):306-314

[4] Falanga V, et al. Autologous bone marrow-derived cultured mesenchymal stem cells delivered in a fibrin spray accelerate healing in murine and human cutaneous wounds. Tissue Engineering. 2007;**13**(6):1299-1312

[5] Badiavas EV, Falanga V. Treatment of chronic wounds with bone marrow-derived cells. Archives of Dermatology. 2003;**139**(4):510-516

[6] Chung E, et al. Fibrin-based stem cell containing scaffold improves the dynamics of burn wound healing. Wound Repair and Regeneration. 2016;**24**(5):810-819

[7] Sanchez-Sanchez R, et al. Generation of two biological wound dressings as a potential delivery system of human adipose-derived mesenchymal stem cells. Asaio Journal. 2015;**61**(6):718-725

[8] Ji SZ, et al. An epidermal stem cells niche microenvironment created by engineered human amniotic membrane. Biomaterials. 2011;**32**(31):7801-7811

[9] Yin Z, et al. The effect of decellularized matrices on human tendon stem/progenitor cell differentiation and tendon repair. Acta Biomaterialia. 2013;**9**(12):9317-9329

[10] Bi Y, et al. Identification of tendon stem/progenitor cells and the role of the extracellular matrix in their niche. Nature Medicine. 2007;**13**(10):1219-1227

[11] Huang SP, et al. Adipose-derived stem cells seeded on acellular dermal matrix grafts enhance wound healing in a murine model of a full-thickness defect. Annals of Plastic Surgery. 2012;**69**(6):656-662

[12] Martinello T, et al. Successful recellularization of human tendon scaffolds using adipose-derived mesenchymal stem cells and collagen gel. Journal of Tissue Engineering and Regenerative Medicine. 2014;**8**(8):612-619

[13] Ouyang HW, et al. Mesenchymal stem cell sheets revitalize nonviable dense grafts: Implications for repair of large-bone and tendon defects. Transplantation. 2006;**82**(2): 170-174

[14] Protzman NM, Stopyra GA, Hoffman JK. Biologically enhanced healing of the human rotator cuff: 8-month postoperative histological evaluation. Orthopedics. 2013;**36**(1):38-41

[15] Altman AM, et al. Human adipose-derived stem cells adhere to acellular dermal matrix. Aesthetic Plastic Surgery. 2008;**32**(4):698-699

[16] Altman AM, et al. Dermal matrix as a carrier for *in vivo* delivery of human adipose-derived stem cells. Biomaterials. 2008;**29**(10):1431-1442

[17] Gao Y, et al. Methodology of fibroblast and mesenchymal stem cell coating of surgical meshes: A pilot analysis. Journal of Biomedical Materials Research Part B Applied Biomaterials. 2014;**102**(4):797-805

[18] Lam MT, et al. Effective delivery of stem cells using an extracellular matrix patch results in increased cell survival and proliferation and reduced scarring in skin wound healing. Tissue Engineering Part A. 2013;**19**(5-6):738-747

[19] Liu S, et al. Synergistic angiogenesis promoting effects of extracellular matrix scaffolds and adipose-derived stem cells during wound repair. Tissue Engineering Part A. 2011;**17**(5-6):725-739

[20] Mifune Y, et al. Tendon graft revitalization using adult anterior cruciate ligament (ACL)-derived CD34+ cell sheets for ACL reconstruction. Biomaterials. 2013;**34**(22):5476-5487

[21] Kato Y, et al. Allogeneic transplantation of an adipose-derived stem cell sheet combined with artificial skin accelerates wound healing in a rat wound model of type 2 diabetes and obesity. Diabetes. 2015;**64**(8):2723-2734

[22] Lee JY, et al. BMP-12 treatment of adult mesenchymal stem cells *in vitro* augments tendon-like tissue formation and defect repair *in vivo*. PLoS One. 2011;**6**(3):e17531

[23] Edwards SS, et al. Functional analysis reveals angiogenic potential of human mesenchymal stem cells from Wharton's jelly in dermal regeneration. Angiogenesis. 2014;**17**(4):851-866

[24] Formigli L, et al. Dermal matrix scaffold engineered with adult mesenchymal stem cells and platelet-rich plasma as a potential tool for tissue repair and regeneration. Journal of Tissue Engineering and Regenerative Medicine. 2012;**6**(2):125-134

[25] Caliari SR, Harley BA. Structural and biochemical modification of a collagen scaffold to selectively enhance MSC tenogenic, chondrogenic, and osteogenic differentiation. Advanced Healthcare Materials. 2014;**3**(7):1086-1096

[26] Cheng XG, et al. Platelet-derived growth-factor-releasing aligned collagen–nanoparticle fibers promote the proliferation and tenogenic differentiation of adipose-derived stem cells. Acta Biomaterialia. 2014;**10**(3):1360-1369

[27] Cheng X, et al. Preparation and *in vitro* evaluation of electrochemically-aligned collagen matrix as a dermal substitute. MRS Advances. 2016;**1**(18):1295-1300

[28] Valencia Mora M, et al. Application of adipose tissue-derived stem cells in a rat rotator cuff repair model. Injury. 2014;**45**(Suppl 4):S22-27

[29] Nambu M, et al. Accelerated wound healing in healing-impaired db/db mice by autologous adipose tissue-derived stromal cells combined with atelocollagen matrix. Annals of Plastic Surgery. 2009;**62**(3):317-321

[30] Rustad KC, et al. Enhancement of mesenchymal stem cell angiogenic capacity and stemness by a biomimetic hydrogel scaffold. Biomaterials. 2012;**33**(1):80-90

[31] Nowacki M, et al. Filling effects, persistence, and safety of dermal fillers formulated with stem cells in an animal model. Aesthetic Surgery Journal. 2014;**34**(8):1261-1269

[32] Hsu SH, Hsieh PS. Self-assembled adult adipose-derived stem cell spheroids combined with biomaterials promote wound healing in a rat skin repair model. Wound Repair and Regeneration. 2015;**23**(1):57-64

[33] Bellini MZ, et al. Combining xanthan and chitosan membranes to multipotent mesenchymal stromal cells as bioactive dressings for dermo-epidermal wounds. Journal of Biomaterials Applications. 2015;**29**(8):1155-1166

[34] Xu K, et al. Thiol-ene Michael-type formation of gelatin/poly(ethylene glycol) biomatrices for three-dimensional mesenchymal stromal/stem cell administration to cutaneous wounds. Acta Biomaterialia. 2013;**9**(11):8802-8814

[35] Xie SY, et al. Adult stem cells seeded on electrospinning silk fibroin nanofiberous scaffold enhance wound repair and regeneration. Journal of Nanoscience and Nanotechnology. 2016;**16**(6):5498-5505

[36] Zhang W, et al. Weft-knitted silk-poly(lactide-co-glycolide) mesh scaffold combined with collagen matrix and seeded with mesenchymal stem cells for rabbit Achilles tendon repair. Connective Tissue Research. 2015;**56**(1):25-34

[37] Garzon I, et al. Wharton's jelly stem cells: a novel cell source for oral mucosa and skin epithelia regeneration. Stem Cells Translational Medicine. 2013;**2**(8):625-632

[38] Rodrigues C, et al. New therapy of skin repair combining adipose-derived mesenchymal stem cells with sodium carboxymethylcellulose scaffold in a pre-clinical rat model. PLoS One. 2014;**9**(5):e96241

[39] Chen S, et al. Mesenchymal stem cell-laden anti-inflammatory hydrogel enhances diabetic wound healing. Scientific Reports. 2015;**5**:18104

[40] Adams Jr SB, et al. Stem cell-bearing suture improves Achilles tendon healing in a rat model. Foot & Ankle International. 2014;**35**(3):293-299

[41] James R, et al. Tendon tissue engineering: Adipose-derived stem cell and GDF-5 mediated regeneration using electrospun matrix systems. Biomedical Materials. 2011;**6**(2):025011

[42] Deng D, et al. Repair of Achilles tendon defect with autologous ASCs engineered tendon in a rabbit model. Biomaterials. 2014;**35**(31):8801-8809

[43] Kim YS, et al. Survivorship of implanted bone marrow-derived mesenchymal stem cells in acute rotator cuff tear. Journal of Shoulder and Elbow Surgery. 2013;**22**(8):1037-1045

[44] Vaquette C, et al. A poly(lactic-co-glycolic acid) knitted scaffold for tendon tissue engineering: An *in vitro* and *in vivo* study. Journal of Biomaterials Science Polymer Edition. 2010;**21**(13):1737-1760

[45] Yokoya S, et al. Rotator cuff regeneration using a bioabsorbable material with bone marrow-derived mesenchymal stem cells in a rabbit model. The American Journal of Sports Medicine. 2012;**40**(6):1259-1268

[46] Fu Y, et al. Human urine-derived stem cells in combination with polycaprolactone/gelatin nanofibrous membranes enhance wound healing by promoting angiogenesis. Journal of Translational Medicine. 2014;**12**:274

[47] Gu J, et al. Adiposed-derived stem cells seeded on PLCL/P123 eletrospun nanofibrous scaffold enhance wound healing. Biomedical Materials. 2014;**9**(3):035012

[48] Biazar E, Keshel SH. The healing effect of stem cells loaded in nanofibrous scaffolds on full thickness skin defects. Journal of Biomedical Nanotechnology. 2013;**9**(9):1471-1482

[49] Zeinali R, et al. Regeneration of full-thickness skin defects using umbilical cord blood stem cells loaded into modified porous scaffolds. ASAIO Journal. 2014;**60**(1):106-114

We are IntechOpen,
the world's leading publisher of Open Access books
Built by scientists, for scientists

6,300
Open access books available

171,000
International authors and editors

190M
Downloads

154
Countries delivered to

Our authors are among the

TOP 1%
most cited scientists

12.2%
Contributors from top 500 universities

CLARIVATE ANALYTICS

BOOK CITATION INDEX

INDEXED

WEB OF SCIENCE™

Selection of our books indexed in the Book Citation Index
in Web of Science™ Core Collection (BKCI)

Interested in publishing with us?
Contact book.department@intechopen.com

Numbers displayed above are based on latest data collected.
For more information visit www.intechopen.com

Natural Rubber Latex Biomaterials in Bone Regenerative Medicine

Leandra E. Kerche-Silva,
Dalita G.S.M. Cavalcante and Aldo Eloizo Job

Additional information is available at the end of the chapter

Abstract

Natural rubber latex (NRL) is a white and milky solution that exudes from *Hevea brasiliensis* bark when perforated, and it has been appointed as a new promising biomaterial. NRL has been proven to be a very biocompatible material, and several new biomedical applications have been proposed. NRL has been proven to stimulate angiogenesis, cellular adhesion and formation of extracellular matrix, besides promoting replacement and regeneration of tissue. NRL also can be used as an occlusive membrane for guided bone regeneration (GBR) with promising results. Therefore, the aim of this chapter is to review NRL studies and to present NRL membrane as a promising biomembrane for use in bone trauma and injury.

Keywords: natural rubber latex, biomembranes, biomaterial, bone regeneration

1. Introduction

Hevea brasiliensis, popularly known as rubber tree, is a plant species that belongs to the Euphorbiaceae family. This plant synthesizes latex by a system of laticiferous rings, organized as paracirculatory vessel systems, in the inner bark of the plant. Latex is the cytoplasm of the laticiferous cells, and its composition resembles the composition of common cells, except for having 30–45% of natural rubber [1]. The latex of *H. brasiliensis* exudes from the bark when it is perforated (**Figure 1**).

Most of the harvested latex is coagulated for the manufacture of "dry rubber" products, including automotive tires. The latex of *H. brasiliensis* can be stabilized in an uncoagulated form with the use of ammonia, which allows the latex to be used for the manufacture of other products, such as surgical gloves (**Figure 2**) [2].

Figure 1. Latex of *Hevea brasiliensis* on exuding of bark after drilling.

Figure 2. Products made by the latex of *Hevea brasiliensis*.

Natural rubber latex (NRL) from *H. brasiliensis* is a colloidal anionic system formed by rubber particles (1,4-*cis*-polyisoprene) stabilized by phospholipids and proteins molecules (**Figure 3**) [4, 5]. One-third of the weight of *H. brasiliensis* latex is made of natural rubber, but 1–2% of its weight consists of hundreds of proteins [5]. Other constituents such as lipids, Quebrachitol, ribonucleic acids and organic salts are also present [6].

In the last years, researchers have been publishing about NRL membranes (**Figure 4**) that has been proven to be an important inductor of wound healing, inductor of esophagic wall regeneration and tympanic membrane regeneration, by mechanisms involved with angiogenesis [7–9]. NRL has also been studied for reconstructing temporal muscle fascia [9] and as arterial prosthesis in animal models, healing of ocular conjunctiva and neoangiogenesis in rabbits [10].

Besides forming biomembranes, which represent a complex colloid made of rubber particles and lutoids bodies suspended in a protein-rich media, NRL can be centrifuged in high speed and separated in fractions that mainly consist of a superior phase of rubber particles, an aqueous phase called centrifuged serum (C-serum) and an inferior phase called bottom serum (B-serum) (**Figure 5**) [12–14].

The rubber particles represent 25–45% of the fresh NRL and they have a medium diameter of 50 Å to 3 μm [15, 16]. The main proteins found in the rubber particles surface are Hev b 1 and Hev b 3 [17]. Centrifuged serum is the solution composed by carbohydrates, electrolytes, proteins and amino acids. This solution is composed by the cytoplasm of the laticiferous cells and contains a great amount of proteins related to the cell metabolism [18]. This phase is implicated with most of the biological properties of NRL [19]. Bottom serum is mainly constituted of lutoids, spherical
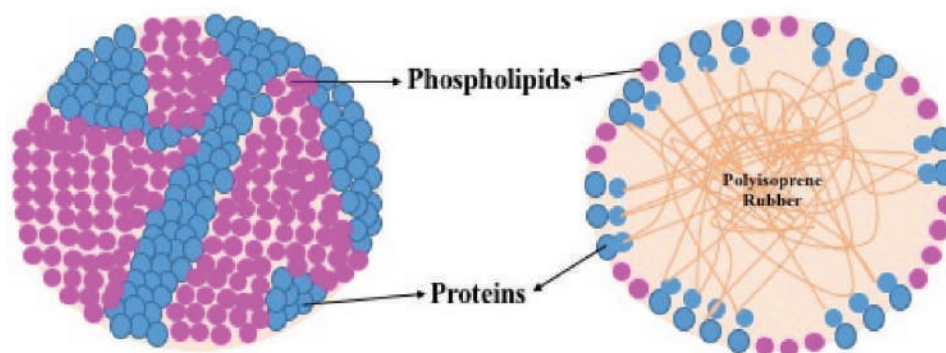

Figure 3. Rubber particles surrounded by a layer of protein-phospholipid (adapted from Ref. [3]).
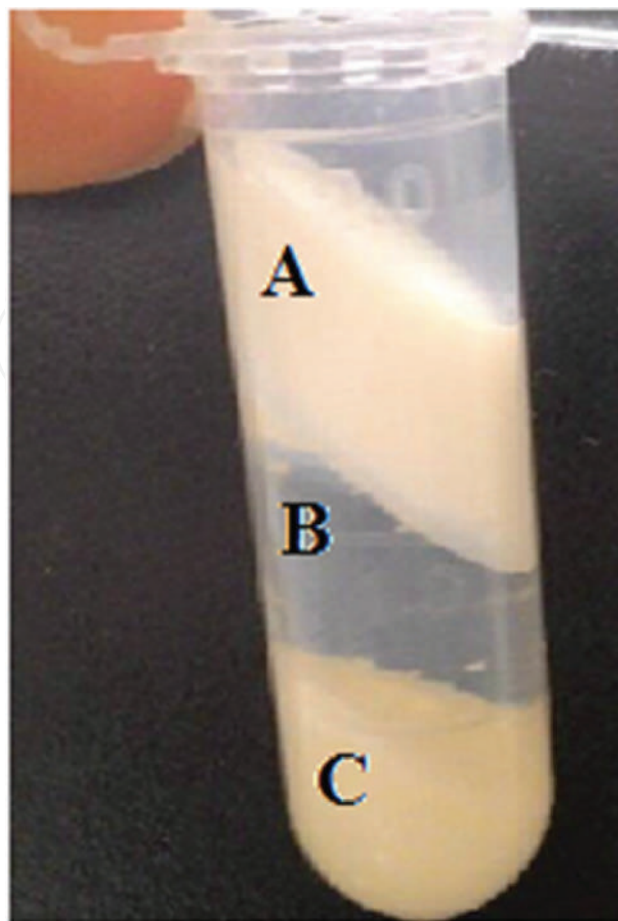

Figure 4. NRL membrane.

Figure 5. NRL fractions after high speed centrifugation: (A) rubber particles, (B) centrifuged serum and (C) bottom serum.

vacuoles that are osmotically sensitive and induce the latex flow to stop [20, 21]. Hevein is the main protein found in bottom serum, and it is implicated with allergenic reactions [18].

Since many biological and biomedical properties can be implicated with NRL from *H. brasiliensis*, the aim of this chapter is to review and explore the studies showing the applications of this biomaterial in bone regenerative medicine.

2. Bone remodeling

Bone is an organ capable of replacing old and disrupted tissue through a remodeling process. Mechanical changes required by skeletal functions make the remodeling process indispensable for the bones. The cells responsible for this process are osteoblasts and osteoclasts, and the first promote bone formation and the latter bone resorption. Osteoblasts are derived of the osteogenic differentiation of mesenchymal stem cells. Other important skeletal cells that have their origin in mature osteoblasts are the osteocytes, and these cells in particular are surrounded by extracellular matrix and have the ability to regulate osteoblast and osteoclast activities to maintain bone homeostasis [11].

Bones protect vital organs and provide storage for calcium and phosphate. Bone compartments designated for mechanical functions are called cortical bone, and the bone compartments designed for metabolic functions are called trabecular bone. Bones can also be distinguished by their formation. When the formation occurs in a direct way, it is called intramembranous ossification and it is characterized by the condensation of mesenchymal stem cells that become osteoblasts. This type of process occurs in the flat bones of neuro- and viscerocranium and in part of the clavicle [22]. When bone formation occurs in an indirect way, it is called endochondral ossification, and it is characterized by the differentiation of mesenchymal stem cells into cartilage first and this cartilage is later replaced by bone [23]. Endochondral ossification occurs in long bones, in vertebrae and in the skull base and the posterior part of the skull [22].

Bone modeling occurs during the growth process, and bone remodeling occurs during lifetime. These two processes take place under the control of various substances such as parathyroid hormone (PTH), calcitonin, vitamin D, growth hormone (GH), steroids, soluble cytokines and growth factors (i.e., macrophage colony-stimulating factor (M-CSF), receptor activator of nuclear κB ligand (RANKL), vascular endothelial growth factor (VEGF) and interleukin-6 (IL-6) family) [11].

Microfractures or factors related to bone microenvironment generate different stimuli that induce osteoblast to produce RANKL, which interacts with its receptor expressed by osteoclasts. This interaction activates the polarization of the osteoclasts that secrets enzymes required for bone resorption. Osteoblasts synthesize type I collagen (that represents 90% of the proteins in bone matrix) and procollagen I N-terminal peptide (PINP) that is considered a marker of bone formation [24].

Type I collagen together with other fibrillar collagens, bone proteins (osteopontin, bone sialoprotein and osteocalcin), proteoglycans, fibronectin and glycosaminoglycans compose unmineralized osteoid. The development of the osteoblast along with the stimulation of the osteogenic genes and mineral deposition are dependent on the pigment epithelium-derived factor (PEDF) [25]. Osteoblast phosphatases are responsible for the mineralization process, since they release phosphates that along with calcium form hydroxyapatite crystals $[Ca_{10}(PO_4)_6(OH)_2]$ [26]. The osteoblasts that remain trapped inside the mineralized matrix acquire a stellar shape after morphologic change and form a network that produces signaling through bone tissue. These cells are called osteocytes.

2.1. Bone formation and bone remodeling molecular pathways

During osteogenesis, bone morphogenetics proteins (BMPs) and WNT signaling pathways are very important. The BMP pathways activate intracellular proteins called SMAD that control the expression of the gene RUNX2 (runt-related transcriptional factor 2), and this gene codifies a transcriptional factor that stimulates the mesenchymal stem cells to differentiate into osteogenic lineage [27]. WNT pathway is formed by proteins that are involved in many other biological processes, and it also regulates the expression of RUNX2 gene [28].

Depending on the level of differentiation of progenitor cells, WNT classic pathway induces or inhibits osteoblast formation. It also controls bone resorption when increasing the ratio of osteoprotegerin (OPG)/RANKL proteins [28]. These proteins are specifically produced by osteoblast

to either inhibit (OPG) or enhance (RANKL) osteoclasts activity [29]. **Figure 6** schematically represents the complex network of molecular signaling pathways during osteogenesis.

Besides the pathways described above, systemic hormones also regulate osteogenic commitment or differentiation of mesenchymal cells. Examples of these hormones are PTH, glucocorticoids and estrogens. Local growth factor signaling, such as bone transforming growth factor-β (TGF-β1/2), insulin-like growth factor (IGF), fibroblast growth factor 2 (FGF-2), VEGF, cytokine modulators (prostaglandins) and mitogen-activated protein kinases (MAPK), also regulates the differentiation of mesenchymal stem cells [30]. Other enzyme that plays an important role in bone regulation is Peptidyl-prolyl *cis-trans* isomerase NIMA-interacting 1 (PIN1), which interacts with RUNX2, SMAD1/5 and ß-catenin proteins [31].

Osteogenesis is also regulated by epigenetic factors such as DNA methylation, microRNAs (miRNAs), histone acetylation and deacetylation, and chromatin structure modification [32, 33]. Especially short noncoding miRNAs have been proven to affect both osteoblast (bone formation) and osteoclast (bone resorption) lineage. Some miRNAs regulate osteoblastogenesis by posttranscription regulation of RUNX2 (e.g., miR-34c, miR-133a, miR135a, miR-137, miR-205, miR-217, etc.), Osterix (OSX) (e.g., miR-31, miR-93, miR-143, miR-145, etc.) and type I collagen (e.g., miR-29, miR-Let7) proteins [34].

After a bone fracture, an inflammatory response is activated and it is crucial for the process of bone regeneration, bone remodeling and healing. This inflammatory response involves the secretion of tumor necrosis factor-α (TNF-α) and interleukins (IL) IL-1, IL-6, IL-11 and IL-18
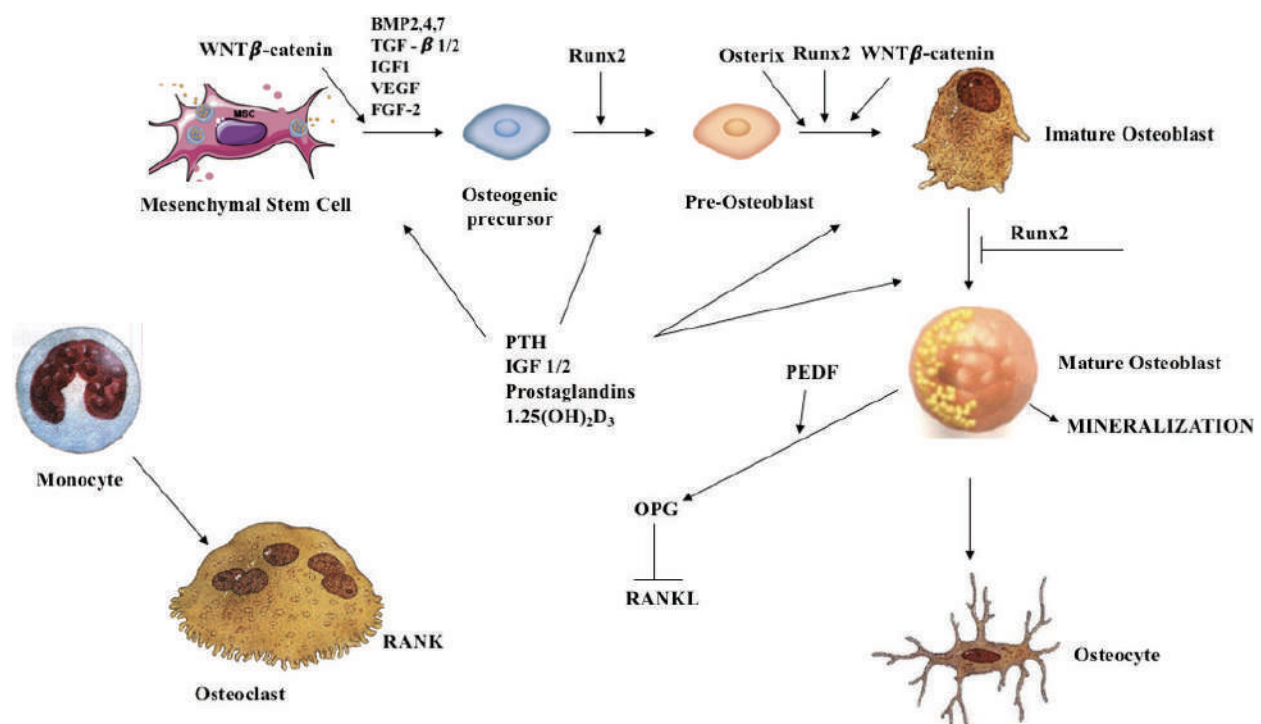

Figure 6. Schematic representation of cells and regulatory molecules involved in osteoblastogenesis and bone formation (adapted from [11]).

by macrophages, inflammatory cells and mesenchymal cells [35]. TNF-α stimulates osteoclast cells and promotes mesenchymal stem cells to start endochondral bone formation. TNF-α also stimulates apoptosis in hypertrophic chondrocytes, and a delay in the reabsorption of mineralized cartilage stops bone formation. When TNF-α is overproduced, as in diabetics, the cartilage is removed in a premature way, delaying bone formation and healing [36]. Right after the injury, during osteoclastogenesis, RANKL and OPG expressions are elevated. In bone remodeling, the expression of these proteins is diminished [37].

During bone remodeling, IL-1 and IL-6 are the most important IL. IL-1 is produced by macrophages and promotes the formation of the primary cartilaginous callus and also promotes angiogenesis in the site [38]. IL-1 also stimulates the production of IL-6 by the osteoblasts, and IL-6 also stimulates angiogenesis by the production of VEGF. It induces the differentiation of osteoblasts and osteoclasts [39].

In bone remodeling, mesenchymal, osteoblasts and chondrocytes cells produce BMPs that can work independently or in collaboration with each other and with other members of the TGF-β family to start osteoclastogenesis [40]. BMPs are structurally and functionally related, but they exhibit different patterns of expression during bone remodeling. Murine studies have shown that BMP-2 expression is more elevated in the first 24 h after the fracture, suggesting its primary function in the beginning of the bone repair. This BMP is also related to the maintenance of the normal bone mass [41, 42].

BMP-3, BMP-4, BMP-7 and BMP-8 are expressed during the healing time (14–21 days after the injury) when there is reabsorption of the calcified cartilage and osteogenesis [43]. It has been proposed that BMP-7 is the most potent inductor of differentiation in mesenchymal stem cells to osteoblasts [44].

2.2. Vasculature involved in bone formation and bone remodeling

Bone is a connective tissue that possesses high vascularization. During bone endochondral and intramembranous ossification, regeneration and remodeling, the vasculature plays an important role [45]. Ten to fifteen percent of total cardiac output goes to skeletal system [46]. The role of the blood vessels in the bone is not only to supply the bones with oxygen and nutrients but also to provide them with growth factor, hormones and neurotransmitters (e.g., brain-derived serotonin), maintaining the bone activity and cell survivor [47, 48].

Osteogenesis can occur through endochondral or intramembranous ossification; in both ways, angiogenesis is a critical stage and it is associated with the production of VEGF by hypertrophic chondrocytes or mesenchymal stem cells, respectively [49]. VEGF attracts endothelial cells acting as a chemotactic molecule that controls differentiation and function of osteoblasts and osteoclasts, participating in bone modeling and bone remodeling. A loss of the VEGF leads to incomplete bone vascularization and automatic disturbed endochondral ossification [50]. On the other hand, overexpression of VEGF can lead to osteosclerosis, highly increased bone formation that is a result of intense osteoblast differentiation, ending in altered bone morphology [51].

In endochondral ossification, cartilage vascularization begins with the formation of a primary vessel that is projected from the perichondrial vascular network to the adjacent cartilage. Then, a capillary glomerulus is formed at the leading edge and the entire vascular unit grows. Following elongation, a backward expansion of the capillary network occurs and it tightly surrounds a pair of main vessels composed by an arteriole and a venule [52].

In intramembranous ossification, capillaries of a small diameter move into thin avascular layer of mesenchyme that surrounds the mesenchymal condensation center. In this center, mesenchymal cells secrete VEGF that attracts endothelial cells. At the start of mineralization of the bone, the first blood vessels associate with an extensive external network of blood vessels [53].

During bone remodeling and bone regeneration, the blood vessels play an important role. Osteoclasts form a cutting cone that moves forward resorbing dead bone or damaged/old bone matrix. A blood vessel follows this cutting cone, delivering nutrients, hormones and growth factors to osteoblast that will produce new bone [48]. OSX-expressing osteoblast precursors are involved in the process of remodeling, accompanying the blood vessels, positioning themselves in a perivascular localization, showing the tight relationship between osteogenesis and angiogenesis [54].

3. Bone remodeling and latex

To clinically manage situations such as bone loss, injury or disease, researchers have been engaged for a long time to find a biocompatible material that is innocuous, promotes osseointegration, is manageable and has low cost for the people who need it. Natural rubber latex (NRL) extracted from *Hevea brasiliensis* has been used in the industrial manufacturing of several products, such as gloves, condoms, balloons and parts of medical and dental equipment [55].

Based on a new manufacturing process, several new biomedical applications have been proposed since NRL has been shown to be very biocompatible, stimulating cellular adhesion, the formation of extracellular matrix, and promoting the replacement and regeneration of tissue [8]. This new manufacturing process is based on the production of a biomembrane of NRL that has been used to replace vessels, esophagus, pericardium and abdominal wall [7]. In all of these experiments, the biomembrane promoted rapid tissue repair and elicited an inflammatory response that resembled the inflammatory response of normal healing process and not one of rejection process [8].

The membrane of NRL was also tested for the repair of bone defects in dental alveoli of rats [56], and the histological examination of the extraction sockets revealed a pattern of normal repair with characteristics similar to those reported for other materials [57]. Histometric evaluation of the areas close to the implant during the initial 7 days demonstrated progressive and accelerated osteogenesis by a decrease in the thickness of the fibrous capsule. At long-term, NRL implants did not induce the formation of foreign-body reaction nor persistent

inflammatory reaction, and after 42 days, the NRL implants were making close contact to the bone at many sites.

The induction of angiogenesis is crucial for bone regeneration and remodeling, and a study using chick embryo chorioallantoic membrane (CAM) showed that NRL membranes possess angiogenic properties. The experiment also showed that the angiogenic capacity of the NRL membranes remains active and increases in temperatures ranging from 65 to 85°C. These results showed that the heating used to prepare NRL membrane does not affect its biological properties. The same study used centrifuged latex to demonstrate that the poly-isoprene is not the part of latex responsible for the biological properties [4].

Large fractures can mean significant reconstructive problems and sometimes require special procedures for regeneration. And this regeneration is dependent on blood clot stability, local vascularization, defect size and protection against invasion of competitive nonosteogenic tissues [58, 59]. Guided bone regeneration (GBR) was a technique developed to enhance bone repair, and in this procedure, an occlusive membrane is used to provide to the osteogenic cells better conditions to perform bone remodeling [60].

Different types of membranes have been tested for use in GBR, but resorbable membranes represent the most interesting alternative since they avoid removal surgery [61]. NRL membranes were tested as an occlusive barrier in GBR of large defects in rabbit calvaria. NRL membranes successfully enhanced bone regeneration process in the group of the treated animals, and it was shown by a statistically higher volume of mature bone in all periods of study that was up to 120 days. The NRL membranes worked as a passive barrier membrane that prevented epithelial and connective tissue migration, thus facilitating the proliferation and migration of regenerative bone cells into the wound. The NRL membranes used for GBR, as well as the ones used to treat dental alveoli defects, did not induce the formation of foreign body inflammatory reaction [62].

Another way to accelerate bone regeneration and remodeling would be incorporating BMPs to NRL membrane. As shown above, BMPs induce bone remodeling and many studies have tried to develop a BMP delivery system that could sustain gradual release of BMPs for dental and orthopedic use [63–66]. A study using bovine serum albumin (BSA) in the place of BMP (same molecular weight) and NRL membranes prepared at different polymerization temperatures showed that NRL membrane was able to release BSA for 18 days. This indicates a promising future of these membranes as active occlusive membrane in GBR and they could release BMPs for 18 days accelerating bone healing [55].

Based on previous studies, a protein was isolated from NRL (P-1) and its inductive bone repair properties were compared to recombinant human bone morphogenetic protein-2 (rhBMP-2), a commercial available human protein with good osteoinductive capabilities. To compare these two proteins, a carrier made of monoolein gel was used. P-1 is still being characterized to better understand its biological properties and its function in the laticifer cells of *Hevea brasiliensis*. However, associated with monoolein gel, P-1 was able to induce new bone formation on bone defect of rat calvaria [67].

This protein extracted from NRL (P-1) was used in combination with a fibrin sealant in the repair of rat tibial bone defects. This combination was successful, being immunoidentified by the presence of osteoblasts in the area, showing high osteogenic and osteoconductive capacity for bone healing [68].

Moura et al. [69] used different polymerized NRL membranes in rabbit calvaria with bone defect. These membranes were compared to polytetrafluoroethylene (PTFE) membranes, which are an extensively studied material considered gold standard for occlusive membranes [70]. In this study, NRL membranes performed their role as biological barriers and achieved a similar performance to the PTFE membrane. One of the polymerized NRL membranes was ammonia free, and these were the membranes that significantly improved the bone repair process producing higher bone formation, being more effective than PTFE membrane. These results were achieved since the method of preparation of these NRL ammonia-free membranes preserved the angiogenic stimulus of the membranes. These membranes also did not lead to bone tissue hypersensitization.

NRL was also coated with calcium phosphate (Ca/P) and tested for biomedical application. Biomaterials added with Ca/P present biological, chemical and mechanical properties very similar to the mineral phase of the bone besides the ability to bond to the host tissue. A hemolytic test was performed, and this material did not affect the blood cells, being so ready for animal tests [71].

These results showed above indicate NRL membranes as a promising future biomembrane that could be used to accelerate bone healing. More experiments are being done already in humans. Since NRL membranes present intense angiogenic activity and wound healing activity, NRL membranes are being commercialized in Brazil and other 60 countries around the world as a band-aid curative (BIOCURE®) for the treatment of ulcers in diabetic patients.

Author details

Leandra E. Kerche-Silva*, Dalita G.S.M. Cavalcante and Aldo Eloizo Job

*Address all correspondence to: leakerche@gmail.com

Department of Physics, Chemistry and Biology, Universidade Estadual Paulista "Júlio de Mesquita Filho", Presidente Prudente, São Paulo, Brazil

References

[1] Jacob JL, Auzac J, Prevôt JL. The composition of natural latex from *Hevea brasiliensis*. Clinical Reviews in Allergy & Immunology. 1993;**11**:325-337

[2] Arif SAM, Hamilton RG, Yusof F, Chew NP, Loke YH, Nimkar S. Isolation and characterization of the early nodule-specific protein homologue (Hev b 13), an allergenic lipolytic esterase from *Hevea brasiliensis* latex. Journal of Biological Chemistry. 2004;**279**:23933-23941

[3] Nawamawat K, Sakdapipanich JT, Ho CC, Ma Y, Vancso JG. Surface nanostructure of *Hevea brasiliensis* natural rubber latex particles. Colloids and Surfaces A. 2011;**390**:157-166

[4] Ferreira M, Mendonça RJ, Coutinho-Netto J, Mulato M. Angiogenic properties of natural rubber latex biomembranes and the serum fraction of *Hevea brasiliensis*. Brazilian Journal of Physics. 2009;**39**:564-569

[5] Rippel MM, Lee L-T, Leite CA, Galembeck F. Skim and cream natural rubber particles: Colloidal properties, coalescence and film formation. Journal of Colloid and Interface Science. 2003;**268**:330-340

[6] Bealing FJ. Quebrachitol synthesis in *Hevea brasiliensis*. Journal of Rubber Research Institute of Malaysia. 1981;**29**:111-112

[7] Mrue F. Neoformação tecidual induzida por biomembranas de latex natural com poli-lisina. Aplicabilidade na neoformação esofágica e da parede abdominal. Estudo experimental com cães [thesis (Doctorate in Medicine, Area: Surgery)]. Ribeirão Preto: Faculdade de Medicina de Ribeirão Preto, Universidade de São Paulo; 2000. p. 111

[8] Mrue F, Coutinho-Netto J, Ceneviva R, Lachat JJ, Thomazini JA, Tambelini H. Evaluation of the biocompatibility of a new biomembrane. Materials Research. 2004;**7**:277-283

[9] Oliveira JAA, Hyppolito MA, Coutinho-Netto J, Mrué F. Miringoplastia com a utilização de um novo material biossintético. Revista Brasileira de Otorrinolaringologia. 2003;**69**:649-655

[10] Pinho ECCM, Souza SJF, Schaud F, Lachat JJ, Coutinho-Netto J. Uso experimental da biomembrane de latex na reconstrução conjunctival. Arquivos Brasileiros de Oftalmologia. 2004;**67**:27-32

[11] Valenti MT, Carbonare LD, Mottes M. Osteogenic differentiation in healthy and pathological conditions. International Journal of Molecular Sciences. 2017;**18**:41-49

[12] Moir GFJ. Ultracentrifugation and staining of *Hevea* latex. Nature. 1959;**184**:1626-1628

[13] Sunderasan E, Rahman NABD, Lam KL, Yang KL, Ong MT. Proteins of dialysed C-serum supernatant sub-fractions elicit anti-proliferative activity on human cancer-origin cells. Journal of Rubber Research. 2015;**18**:49-59

[14] Yeang HY. Characterisation of rubber particle destabilization by B-serum and Bark Sap of *Hevea brasiliensis*. Journal of Natural Rubber Research. 1988;**4**:47-55

[15] Gomez JB, Moir GK. The ultracytology of latex vessels in *Hevea brasiliensis*. Monograph No. 4. Kuala Lumpur: Malaysian Rubber Research and Development Board; 1979

[16] Schoon THGF, Phoa KL. Morphology of the rubber particles in natural lattices. Arch van der Rubberc. 1956;**33**:195

[17] Rolland JM, O'Hehir RE. Latex allergy: A model for therapy. Clinical & Experimental Allergy. 2008;**38**:989-912

[18]   Yeang HY. Allergenic proteins of natural rubber latex. Methods. 2002;**27**:32-45

[19]   Kerche-Silva LE, Cavalcante DGSM, Danna CS, Gomes AS, Carrara IM, Cecchini AL, et al. Free-radical scavenging properties and cytotoxic activity evaluation of latex C-serum from *Hevea brasiliensis* RRIM 600. Free Radicals and Antioxidants. 2017;**7**:107-114

[20]   Dickenson PB. Electron microscopical studies of latex vessel system of *Hevea brasiliensis*. Journal of Rubber Research Institute of Malaysia. 1969;**21**:543-559

[21]   Southorn WA. Complex particles in *Hevea* latex. Nature. 1960;**188**:165-166

[22]   Berendsen AD, Olsen BR. Bone development. Bone. 2015;**80**:14-18

[23]   Wang Y, Li YP, Paulson C, Shao JZ, Zhang X, Wu M, Chen W. Wnt and Wnt signalling pathway in bone development and disease. Frontiers in Bioscience. 2014;**19**:379-407

[24]   Li M, Li Y, Deng W, Zhang Z, Deng Z, Hu Y, et al. Chinese bone turnover marker study: Reference ranges for C-terminal telopeptide of type I collagen and procollagen I N-terminal peptide by age and gender. PLoS One. 2014;**9**:e103841

[25]   Li F, Song N, Tombran-Tink J, Niyibizi C. Pigment epithelium-derived factor enhances differentiation and mineral deposition of human mesenchymal stem cells. Stem Cells. 2013;**31**:2714-2723

[26]   Valenti MT, Carbonare LD, Mottes M. Hypophosphatasia and mesenchymal. International Journal of Stem Cell Research & Therapy. 2016;**3**:20

[27]   Cao X, Chen D. The BMP signaling and *in vivo* bone formation. Gene. 2005;**357**:1-8

[28]   Williams BO, Insogna KL. Where Wnts went: The exploding field of Lrp5 and Lrp6 signaling in bone. Journal of Bone and Mineral Research. 2009;**24**:171-178

[29]   Honma M, Ikebuchi Y, Kariya Y, Suzuki H. Regulatory mechanisms of RANKL presentation to osteoclast precursors. Current Osteoporosis Reports. 2014;**12**:115-120

[30]   Dalle Carbonare L, Innamorati G, Valenti MT. Transcription factor Runx2 and its application to bone tissue engineering. Stem Cell Reviews. 2012;**8**:891-897

[31]   Islam R, Yoon WJ, Ryoo HM, Pin1, the master orchestrator of bone cell differentiation. Journal of Cellular Physiology. 2017;**232**:2339-2347

[32]   Cantley MD, Zannetino ACW, Bartold PM, Fairlie DP, Haynes DR. Histone deacetylases (HDAC) in physiological and pathological bone remodelling. Bone. 2017;**95**:162-174

[33]   Zaidi SK, Young DW, Montecino M, van Wijnen AJ, Stein JL, Lian JB, Stein GS. Bookmarking the genome: Maintenance of epigenetic information. Journal of Biological Chemistry. 2015;**286**:18355-18361

[34]   Jing D, Hao J, Shen Y, Tang G, Li ML, Huang SH, Zhao ZH. The role of microRNAs in bone remodeling. International Journal of Oral Science. 2015;**7**:131-143

[35]   Gerstenfeld LC, Cullinane DM, Barnes GL. Fracture healing as a post-natal developmental process: Molecular, spatial, and temporal aspects of its regulation. Journal of Cellular Biochemistry. 2003;**88**:873-884

[36] Kayal RA, Tsatsas D, Bauer MA, Allen B, Al-Sebaei MO, Kakar S, et al. Diminished bone formation during diabetic fracture healing is related to the premature resorption of cartilage associated with increased osteoclast activity. Journal of Bone and Mineral Research. 2007;**22**:560-568

[37] Gerstenfeld LC, Cho TJ, Kon T, Aizawa T, Tsay A, Fitch J, et al. Impaired fracture healing in the absence of TNF-alpha signaling: The role of TNF-alpha in endochondral cartilage resorption. Journal of Bone and Mineral Research. 2003;**18**:1584-1592

[38] Lee SK, Lorenzo J. Cytokines regulating osteoclast formation and function. Current Opinion in Rheumatology. 2006;**18**:411-418

[39] Yang X, Ricciardi BF, Hernandez-Soria A, Shi Y, Camacho NP, Bostrom MPG. Callus mineralization and maturation are delayed during fracture healing in interleukin-6 knockout mice. Bone. 2007;**41**:928-936

[40] Reddi AH. Bone morphogenetic proteins: From basic science to clinical applications. Journal of Bone and Joint Surgery. American Volume. 2001;**83-A**:S1–S6

[41] Tsuji K, Bandyopadhyay A, Harfe BD, Cox K, Kakar S, Gerstenfeld L, et al. BMP2 activity, although dispensable for bone formation, is required for the initiation of fracture healing. Nature Genetics. 2006;**38**:1424-1429

[42] Xiong DH, Shen H, Zhao LJ, Xiao P, Yang TL, Guo YF, et al. Robust and comprehensive analysis of 20 osteoporosis candidate genes by very high-density single nucleotide polymorphism screen among 405 white nuclear families identified significant association and gene-gene interaction. Journal of Bone and Mineral Research. 2006;**21**:1678-1695

[43] Cho TJ, Gerstenfeld LC, Einhorn TA. Differential temporal expression of members of the transforming growth factor beta superfamily during murine fracture healing. Journal of Bone and Mineral Research. 2002;**17**:513-520

[44] Bais MV, Wigner N, Young M, Toholka R, Graves DT, Morgan EF, et al. BMP2 is essential for post natal osteogenesis but nor for recruitment of osteogenic stem cells. Bone. 2009;**45**:254-266

[45] Filipowska J, Tomaszewski KA, Niedźwiedzki Ł, Walocha JA, Niedźwiedzki T. The role of vasculature in bone development, regeneration and proper systemic functioning. Angiogenesis. 2017

[46] Tomlinson RE, Silva MJ. Skeletal blood flow in bone repair and maintenance. Bone Research. 2013;**1**:314-322

[47] Brandi ML, Collin-Osdoby P. Vascular biology and the skeleton. Journal of Bone and Mineral Research. 2006;**21**:183-192

[48] Niedźwiedzki T, Filipowska J. Bone remodeling in the context of cellular and systemic regulation: The role of osteocytes and the nervous system. Journal of Molecular Endocrinology. 2015;**55**:R23-R26

[49] Liu Y, Olsen BR. Distinct VEGF functions during bone development and homeostasis. Archivum Immunologiae et Therapiae Experimentalis (Warsz). 2014;**62**:363-368

[50] Hu K, Olsen BR. Osteoblast-derived VEGF regulates osteoblast differentiation and bone formation during bone repair. Journal of Clinical Investigation. 2016;**126**:509-526

[51] Maes C, Goossens S, Bartunkova S, Drogat B, Coenegrachts L, Stockmans I, Haigh JJ. Increased skeleton VEGF enhances beta-catenin activity and results in excessively ossified bones. EMBO Journal. 2010;**29**:424-441

[52] Skawina A, Litwin JA, Gorczyca J, Miodoński A. Blood vessels in epiphyseal cartilage of human fetal femoral bone: A scanning electron microscopic study of corrosion casts. Anatomy and Embryology. 1994;**189**:457-462

[53] Thompson TJ, Owens PD, Wilson DJ. Intramembranous osteogenesis and angiogenesis in the chick embryo. Journal of Anatomy. 1989;**166**:55-65

[54] Maes C, Kobayashi T, Selig MK, Torrekens S, Sanford I, Mackem S, Kronenberg HM. Osteoblast precursors, but not mature osteoblasts, move into developing and fractured bones along with invading blood vessels. Developmental Cell. 2010;**19**:329-344

[55] Herculano RD, Pereira Silva C, Ereno C, Guimaraes SAC, Kinoshita A, Graeff CFO. Natural rubber latex used as drug delivery system in guided bone regeneration (GBR). Materials Research. 2009;**12**:253-256

[56] Balabanian CACA, Coutinho-Netto J, Lamano-Carvalho TL, Lacerda SA, Brentegani LG. Biocompatibility of natural latex implanted into dental alveolus of rats. Journal of Oral Science. 2006;**48**:201-205

[57] Brentegani LG, Bombonato KF, Lamano-Carvalho TL. Histologic evaluation of the biocompatibility of glass-ionomer cement in rat alveolus. Biomaterials. 1997;**18**:137-140

[58] Melcher AH, Dreyer CJ. Protection of the blood clot in healing circumscribed bone defects. Journal of Bone and Joint Surgery. British Volume. 1964;**44**:424-430

[59] Schenk RK. Bone regeneration biologic basis. In: Buser D, Dahlin C, Schenk RK, editors. Guided Bone Regenerations in Implant Dentistry. Chicago: Quintessence; 1994. pp. 49-100

[60] Linde A, Alberius P, Dahlin C, Bjurstam K, Sundin Y. Osteopromotion: A soft-tissue exclusion principle using a membrane for bone healing and bone neogenesis. Journal of Periodontology. 1993;**64**:1116-1128

[61] Barber D, Lignelli J, Smith BM, Bartee BK. Using a dense PTFE membrane without primary closure to achieve bone and tissue regeneration. Journal of Oral and Maxillofacial Surgery. 2007;**65**:748-752

[62] Ereno C, Guimarães SAC, Pasetto S, Herculano RD, Pereira Silva C, Graeff CFO, et al. Latex use as an occlusive membrane for guided bone regeneration. Journal of Biomedical Materials Research Part A. 2010;**95A**:932-939

[63] Jung RE, Glauser R, Schärer P, Hämmerle CHF, Sailer HF, Weber FE. Effect of rhBMP-2 on guided bone regeneration in humans: A randomized, controlled clinical and histo-morphometric study. Clinical Oral Implants Research. 2003;**14**:556-568

[64] Müller F, Roher H, Vogel-Höpker A. Bone morphogenetic proteins specify the retinal pigment epithelium in the chick embryo. Development. 2007;**134**:3483-3493

[65] Oshin AO, Stewart MC. The role of bone morphogenetic proteins in articular cartilage development, homeostasis and repair. Veterinary and Comparative Orthopaedics and Traumatology. 2007;**20**:151-158

[66] Woo BH, Fink BF, Page R, Schrier JA, Woo JY, Jiang G, et al. Enhancement of bone growth by sustained delivery of recombinant human bone morphogenetic protein-2 in a polymeric matrix. Pharmaceutical Research. 2001;**18**:1747-1753

[67] Issa JPM, Defino HLA, Coutinho-Netto J, Volpon JB, Regalo SCH, Iyomasa MM, et al. Evaluation of rhBMP-2 and natural latex as potential osteogenic proteins in critical size defects by histomorphometric methods. Anatomical Record. 2010;**293**:794-801

[68] Machado EG, Issa JPM, Figueiredo FAT, Santos GR, Galdeano EA, Alves MC, et al. A new heterologous fibrin sealant as scaffold to recombinant human bone morphogenetic protein-2 (rhBMP-2) and natural latex proteins for the repair of tibial bone defects. Acta Histochemica. 2015;**117**:288-296

[69] Moura JML, Ferreira JF, Marques L, Holgado L, Graeff CFO, Kinoshita A, Comparison of the performance of natural latex membranes prepared with different procedures and PTFE membrane in guided bone regeneration (GBR) in rabbits. Journal of Mater Science: Materials in Medicine. 2014;**25**:2111-2120

[70] Lindhe J, Karring T, Lang NP. Clinical Periodontology and Implant Dentistry. 5th ed. Oxford: Wiley-Blackwell; 2008

[71] Borges FA, Almeida Filho E, Miranda MCR, Santos ML, Herculano RD, Guastaldi AC, Natural rubber latex coated with calcium phosphate for biomedical application. Journal of Biomaterials Science. Polymer edition. 2015;**26**:1256-1268